Effect of ceramide composition on stratum corneum structure - a molecular dynamics study

Natalia Rivero Arenas

Trabajo de Grado para Optar al Título de Magister en Química

Directora

Martha Cecilia Daza Espinosa

Dra. en Ciencias - Química

Codirector

Markus Hans Oliver Doerr

Dr. rer. nat.

Universidad Industrial de Santander

Facultad de Ciencias

Escuela de Química

Maestría en Química

Bucaramanga

2022

Dedication

To my parents, my sister and all those who have believed in me. You make it possible for me to sing these verses identified and happy:

"Y no es tanto lo que pide, es sólo un poco, es el principio, el primer paso que le ayude a caminar. Y así, de paso a pasito ella va abriéndose el camino.
Cuando arranque nadie la podrá parar.

Canta, la esperanza canta y con el tiempo, la tristeza cambia como cambia el aguacero con los vientos.
Canta, que la vida aprieta, pero abraza al que con empeño alza sus alas en el viento y se echa a andar".

-Marta Gómez.

Acknowledgments

I wish to present a very special thanks to my research directors, Prof. Dr. Martha Cecilia Daza Espinosa and Prof. Dr. Markus Hans Oliver Doerr for their orientation and guidance during the whole process.

This work would not have been possible without the financial support of the Universidad Industrial de Santander with the project 1689 of the Internal Call for Research "*Generando Espíritu Científico – Investigación Básica*" and the scholarship provided by the Postgraduate Department.

I would like to express my eternal gratitude to my parents, José Calixto and Amelia, my sister, María Lucía, and to all the great friends that my time at the university has left me. You have been my support and motivation in every step.

Table of Contents

Pag.

List of Tables

Pag.

List of Figures

Pag.

List of Appendices

Pag.

Resumen

Título: Efecto de la composición de ceramidas en la estructura del estrato córneo - un estudio de dinámica molecular*

Autor: Natalia Rivero Arenas**

Palabras Clave: Ceramidas, simulación, matriz extracelular lipídica.

Descripción:

En algunas enfermedades dérmicas con una evidente deshidratación y descamación de la piel, la relación natural de CER[NP]:CER[AP] se altera en la matriz extracelular del estrato córneo aumentando la concentración de CER[AP]. La matriz extracelular del estrato córneo está compuesta por varias bicapas lipídicas apiladas. Hay pocos estudios estructurales de este sistema. En este trabajo grado se estudiaron dos modelos de tres bicapas lipídicas apiladas de CER[NP], CER[AP], colesterol y ácido lignocérico mediante simulaciones de dinámica molecular. Se evaluó el efecto de las proporciones CER[NP]:CER[AP] 1:2 y 2:1 sobre las propiedades estructurales de la matriz extracelular del estrato córneo. Estas propiedades fueron: grosor, ángulo de inclinación de las cadenas acilo, ubicación de los terminales CH_3 de las cadenas acilo y los enlaces de hidrógeno. En la relación CER[NP]:CER[AP] 1:2 se encontró una mayor inclinación y un menor solapamiento entre las cadenas acilo de las dos hemicapas de una bicapa lipídica. Y un mayor grosor de las bicapas lipídicas. El número total de enlaces de hidrógeno presentes en los dos modelos es similar. La CER[AP] forma un mayor número de enlaces de hidrógeno entre el hidroxilo del ácido graso y el agua que entre el hidroxilo 3 de la CER[NP]. Los resultados demuestran que usar un modelo de tres bicapas lipídicas apiladas es mejor, puesto que los obtenidos son similares a los resultados experimentales reportados por Schmitt et al., (2018).

---

* Trabajo de Grado

**Facultad de Ciencias. Escuela de Química. Maestría en Química. Directora: Martha Cecilia Daza Espinosa. Dra. en Ciencias - Química. Codirector: Markus Hans Oliver Doerr. Dr. rer. nat.

Abstract

Title: Effect of ceramide composition on stratum corneum structure - a molecular dynamics study*

Author(s): Natalia Rivero Arenas**

Key Words: Ceramides, simulation, lipid extracellular matrix.

Description:

In some dermal diseases with evident skin dehydration and desquamation, the natural ratio of CER[NP]:CER[AP] is altered in the extracellular matrix of the stratum corneum by increasing the concentration of CER[AP]. The extracellular matrix of the stratum corneum is composed of several stacked lipid bilayers. There are few structural studies of this system. In this graduate work, two models of three stacked lipid bilayers of CER[NP], CER[AP], cholesterol and lignoceric acid were studied by molecular dynamics simulations. The effect of 1:2 and 2:1 CER[NP]:CER[AP] ratios on the structural properties of the stratum corneum extracellular matrix was evaluated. These properties were: thickness, angle of inclination of the acyl chains, location of the CH_3 termini of the acyl chains and hydrogen bonds. In the ratio CER[NP]:CER[AP] 1:2, a greater tilt and a smaller overlap between the acyl chains of the two hemilayers of a lipid bilayer were found. And a greater thickness of the lipid bilayers. The total number of hydrogen bonds present in the two models is similar. CER[AP] forms a greater number of hydrogen bonds between the hydroxyl of the fatty acid and water than between the 3-hydroxyl of CER[NP]. The results show that using a three stacked lipid bilayer model is better, since those obtained are similar to the experimental results reported by Schmitt et al., (2018).

---

* Degree Work

**Facultad de Ciencias. Escuela de Química. Maestría en Química. Director: Martha Cecilia Daza Espinosa. Dra. en Ciencias - Química. Codirector: Markus Hans Oliver Doerr. Dr. rer. nat.

Introduction

The stratum corneum, the outermost layer of the epidermis, is a tissue composed of corneocytes surrounded by an extracellular lipid matrix composed mainly of ceramides (CERs), cholesterol (CHOL) and free fatty acids (FFA) (Das Chinmay & Olmsted Peter D., 2016; Uchida & Park, 2016). Due to the organization of corneocytes, stacked and without interstices, as well as the properties of the lipid matrix surrounding these cells, the stratum corneum is the layer responsible for the barrier function of the skin (van Smeden, Janssens, Gooris, et al., 2014). The extracellular lipid matrix of the stratum corneum is essential for human survival, as it acts as a barrier that prevents rapid dehydration and protects the body against viruses, bacteria, and UV radiation (Elias, 2012).

So far, there are only a few notions about the three-dimensional organization of extracellular lipids in the stratum corneum. However, the role of individual lipid subclasses, the correlation between functionality, composition and structure in healthy and diseased skin remains incomplete. Obstacles such as the complexity and wide chemical variability of lipids present in the stratum corneum, ethical issues related to the use of biological material such as excised human skin, hinder the elucidation of the morphology of this lipid matrix (Lavrijsen et al., 1995).

The lipid matrix surrounding the stratum corneum cells in skin with diseases such as psoriasis, atopic dermatitis, lamellar ichthyosis, among others, shows changes in the organization and proportion of some of their constituent ceramides, for example, in patients with these pathologies, who are characterized by exhibiting evidently dehydrated skin with frequent desquamation (Bouwstra & Ponec, 2006), the concentration of ceramide N-(tetracosanoyl)-phytosphingosine (CER[NP]) decreases, while the concentration of ceramide N-(α-d-

hydroxytetracosanoyl)-phytosphingosine (CER[AP]) increases (Bouwstra & Ponec, 2006; Motta et al., 1993; Pilgram et al., 2001), these ceramides differ only in an additional OH group in the fatty acid chain of CER[AP]. Understanding at the atomic level the effect of the change in the CER[NP]:CER[AP] ratio on the structure of the stratum corneum lipid matrix will enable the future development of effective dermal and transdermal drug delivery strategies to improve skin health in patients with ichthyosis or other related skin diseases.

Recent research used neutron diffraction in combination with specifically deuterated ceramides to study the effect of 1:2 and 2:1 CER[NP]:CER[AP] ratios. They found that the acyl chains of the lipids in one monolayer overlapped with the acyl chains of the lipids in the other monolayer. At the ratio CER[NP]:CER[AP] 1:2 the lipid acyl chains were tilted, and their overlap was reduced, without influencing the bilayer thickness. Whereas, in the CER[NP]:CER[AP] 2:1 ratio the acyl chains were arranged mostly straight with one with a large region of overlap (Schmitt, Lange, et al., 2018). The conformations they propose in this study are hypotheses that explain the experimental results, but it is not yet completely clear how these tilted structures are formed, nor is there the effect of this arrangement on the microscopic structure and interactions in this type of molecular arrangement.

Due to the limited resolution of this experiment, the neutron wavelength was 4.6 Å, the structural information was obtained one-dimensionally, perpendicular to the bilayers (Schmitt, Lange, et al., 2018), the molecular causes of the observed structural changes were not found. Therefore, molecular dynamics simulations offer an atomic-level approach to the detailed study of the three-dimensional structure of the lipid matrix surrounding the corneocytes that it allows to study. So far, simulation studies have provided considerable insight into the effect of the chain length of CERs, the addition of other lipids and the permeation of small molecules on the properties

of lipid bilayers that constitute the extracellular matrix of the stratum corneum (Das et al., 2009; Gupta et al., 2016; Regno & Notman, 2018; Schmitt et al., 2017; Schmitt, Gupta, et al., 2018).

Therefore, the objective of this research was to study by molecular dynamics simulations two models of three stacked lipid bilayers composed of CER[NP], CER[AP], lignoceric acid (LA) and CHOL to analyze the structural differences between the bilayers that are in contact with an external aqueous medium and the middle bilayer, to determine the effect of the 1:2 and 2:1 ratio CER[NP]:CER[AP] on the structural properties and to analyze in more detail the observations made by Schmitt et al., (2018) and compare with our previous studies performed with a lipid bilayer (Rivero, 2019).

1. Objectives

1.1. General Objective

To evaluate the effect of ceramide composition on the structural properties of two models of the stratum corneum lipid matrix.

1.2. Specific Objectives

To determine the effect of 1:2 and 2:1 ratios of CER[NP] and CER[AP] ceramides in two models of three stacked bilayers of the stratum corneum lipid matrix including lignoceric acid and cholesterol.

To characterize the stabilizing interactions in two models of three stacked bilayers of the stratum corneum lipid matrix including lignoceric acid and cholesterol.

To evaluate the effect of the number of lipid bilayers on the structural characteristics of models of the stratum corneum lipid matrix composed of CER[NP], CER[AP], lignoceric acid and cholesterol.

2. Theoretical Framework

2.1. Stratum corneum

The stratum corneum is the outermost layer of the skin. It represents the body's main interface with its environment; therefore, it functions as a barrier, protecting cells and internal tissues from external aggressions while maintaining normal cellular functions. It also limits water loss from the skin (Elias, 2005). It is typically 10-20 μm thick and is composed of 10-15 layers of corneocytes (Menon et al., 2012). Corneocytes are dead cells derived from differentiated keratinocytes that have originated in the deeper layers of the epidermis. Morphologically, corneocytes are flattened and elongated, measuring about 0.2 μm wide and 40-60 μm long (Kashibuchi et al., 2002). They occupy an area of 700-1200 μm^2; thus, there are approximately 105 cells per cm^2. They form a tightly packed set of interdigitated cells, which facilitates the formation of cohesive sheets, that are the cells stacked in vertical columns (Uchida & Park, 2016). Each cell is contained within a primarily protein envelope rather than the conventional lipid bilayer cell membrane. This envelope provides the stratum corneum with most of its mechanical strength, through intracellular keratin disulfide bonds and through the attachment of cells that are embedded in a lipid-enriched extracellular matrix (Boncheva, 2012; Elias, 2012; Matoltsy, 1976).

Ceramides, cholesterol, and free fatty acids are the major components of the extracellular matrix (Das Chinmay & Olmsted Peter D., 2016). Ceramide metabolites, sphingosine and ceramide-1-phosphate, are present as minor components (Goto-Inoue et al., 2012), as well as phospholipids (Elias, 2012). Ceramides account for approximately 50% by mass of stratum corneum lipids and 15 classes, comprising 342 individual species, have been identified (Masukawa et al., 2008). The lipid composition of the stratum corneum varies according to anatomical site

(Lampe et al., 1983), age (Starr et al., 2016), sebaceous gland density (Ludovici et al., 2018) and UV exposure (Wefers et al., 1991).

2.2. Ceramides

Ceramides are the main lipid constituent of the extracellular matrix of the stratum corneum, playing a key role in structuring and thus maintaining the barrier function of the skin. They are a structurally heterogeneous group of sphingolipids and consist of a long-chain fatty acid linked to the amino group of a di- or trihydroxy sphingoid base, sphingosine, phytosphingosine or 6-hydroxysphingosine. The fatty acid bound to the sphingoid base consists predominantly of a very long saturated alkyl chain and may be hydroxylated at the α-position to the carbonyl oxygen, at the end of the hydrocarbon chain, ω-position, or present no hydroxyl group at all (Castro et al., 2014; van Smeden, Janssens, Gooris, et al., 2014).

The nomenclature of ceramides is based on their chemical structure as seen in Figure 1. The first letter defines the type of fatty acid modification present. The [N] represents a non-hydroxylated fatty acid, the [A] an α-hydroxylated fatty acid, the [O] an ω-hydroxylated fatty acid. An [O] CER may additionally be esterified with another fatty acid at the ω-position indicated by an [EO]. The last letter, which is the third letter for [EO], defines the type of sphingoid base. The [S] is for sphingosine, [P] for phytosphingosine, and [H] for 6-hydroxysphingosine. Only dihydrosphingosine is indicated by two letters [DS] (Motta et al., 1993).

Figure 1

Explanation of CER subclasses and CER chain length. CERs are composed of a fatty acid chain linked to a sphingosine base. Both chains show a wide distribution in their carbon chain length (indicated by the arrows). This results in a wide range of the total carbon chain length of CERs.

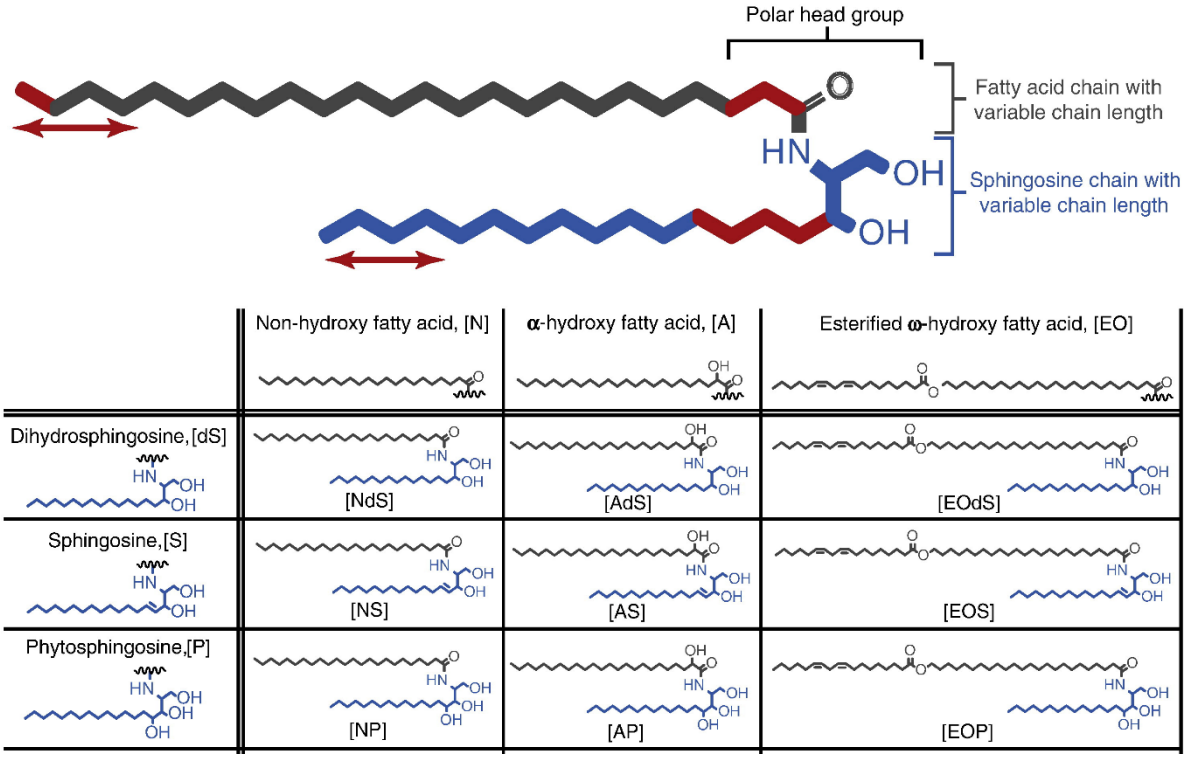

Note Taken from van Smeden, Janssens, Gooris y Bouwstra (2014).

Compared to other lipids such as phospholipids, the head groups of ceramides are smaller and less polar. However, they exhibit strong and stable interactions through a complex network of hydrogen bonds (L. Li et al., 2002). It has been observed that the more hydroxyl groups the head groups of ceramides have the stronger the interaction (Janssens et al., 2009). The α-ceramides, seem to be an exception to this rule, in this case, the additional OH group seems to disrupt the hydrogen bonding network rather than strengthen it. The most abundant α-ceramide in the stratum corneum lipid matrix is CER[AP] (Masukawa et al., 2008). In the native stratum corneum lipid matrix, only the D(2R) isomer of CER[AP] is found (L. Li et al., 2002).

2.3. Structure of the extracellular lipid matrix of the stratum corneum

In contrast to the dermis in which the extracellular matrix is filled with collagen, elastin, glycosaminoglycans and glycoproteins (Bouwstra et al., 2000), the extracellular matrix of the

stratum corneum is composed of long-chain ceramides, free fatty acids, and cholesterol. The extracellular matrix of the stratum corneum shows a unique lamellar arrangement, which differs from that presented by other biological membranes containing mainly phospholipids (Bouwstra et al., 2021; van Smeden, Janssens, Gooris, et al., 2014).

Figure 2 shows schematically the possible chain conformations and lateral packing arrangements of lipid bilayers. In the orthorhombic (OR) phase, which is the densest phase, the lipid chains are arranged in a rectangular crystal lattice with no rotational or translational mobility. In the hexagonal phase (HEX), also called the gel phase, lipid chains are tilted and form a less dense hexagonal lattice; lipid molecules have some rotational mobility, but their translational mobility is restricted. In the liquid crystalline phase (LIQ), the chains show a high degree of gauche isomerization, and lateral organization is completely lost; lipid molecules have high rotational and translational mobility. All three lipid phases are present in the stratum corneum lipid lamellae, with a marked prevalence of the OR phase (Boncheva, 2012). In the direction perpendicular to the surface of the corneocytes, the lipid bilayers are stacked one on top of the other and form a repeating pattern of structural units, lamellae. In the lipid matrix of the stratum corneum there are two types of lamellar structures, which are differentiated by their repeating distance, i.e., by their thickness, one with a thickness of about 13 nm, which is called the long periodicity phase (LPP), and another with a thickness of about 6 nm, which is called the short periodicity phase (SPP) (Schmitt & Neubert, 2018). Shorter SPP arrangements around 4–4.5 nm were also reported (Al-Amoudi et al., 2005).

Figure 2

Schematic presentation of lipid matrix organization in stratum corneum. (a) The stratum corneum is composed of corneocytes surrounded by a lipid matrix, referred to as the brick-and-mortar structure. (b) The corneocytes are covered by a cornified envelope. A monolayer of lipids (bound lipids) is attached to this cornified envelope. The free lipids adopt two lamellae phases, the long periodicity phase (LPP) shown in (c), and the short periodicity phase (SPP)

shown in (d). The lipids within the lamellae assemble in (e) either a liquid (loose packing), a hexagonal (dense packing) or an orthorhombic packing (very dense packing).

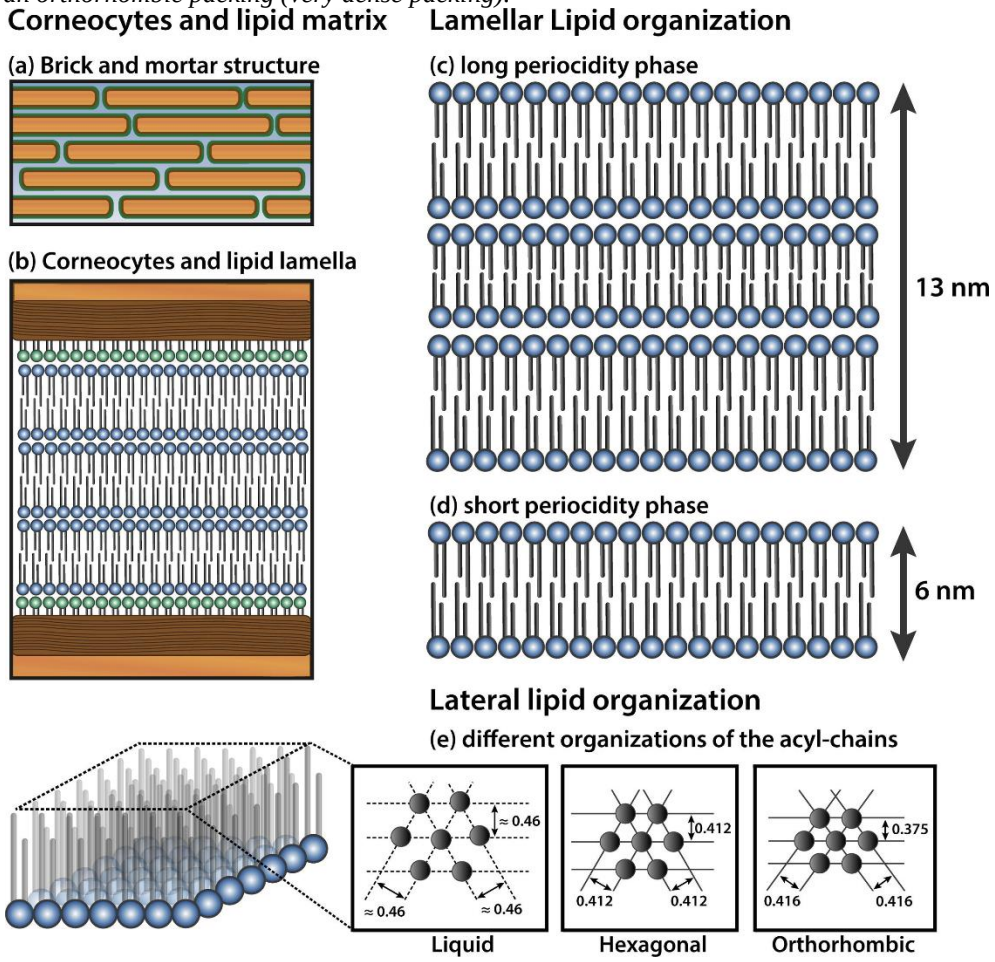

Note Taken from Bouwstra et al., (2021).

2.3.1. Stratum corneum ceramides in diseased skin

All skin conditions are related to alterations in the composition and metabolism of skin lipids and show impaired barrier function (Bouwstra & Ponec, 2006; Paige et al., 1994; Sahle et al., 2015). However, the links between skin disorders and specific lipid concentrations can be difficult to define because of the diverse range of lipid molecules available, especially ceramides (Schmitt & Neubert, 2018). Other skin components, mainly water and proteins, must also be considered. Table 1 presents a summary of trends common to different skin diseases, e.g., decreased total CERs concentrations.

Table 1

Summary of changes in stratum corneum diseases and conditions.

Skin Disease/Condition	Ceramides and Derivatives	
	General trends	
	↓ Total ceramides ↑ Short-chain ceramides ↓ Long-chain ceramides ↑ CER [AP] ↓ CER [NP] (Imokawa et al., 1991; S. Li et al., 2016; Matsumoto et al., 1999)	
	Specific trends	
Atopic Dermatitis	↑ CER[NS] (children) (Shen et al., 2018) ↑ CER[AS] (children) (Shen et al., 2018) ↑ CER36 [NS] (male and female) (Agrawal et al., 2018)	↓ CER[EOS] (Motta et al., 1993) ↓ Acylceramides (Yamamoto et al., 1991)
Psoriasis	↑ Ceramides C12:0, C16:0, C18:0, C18:1, C24:0 and C24:1 (Checa et al., 2015)	
Acne		↓ Average ceramide chain length (Zhou et al., 2018)
Lamellar Ichthyosis	↑ Short-chain ceramides (Lavrijsen et al., 1995)	✗ ceramides with very long acyl chains (C26 - C34) ↓ acyl-CERs (subgroup of patients) (Paige et al., 1994)
Netherton Syndrome	↑ C34 CERs of subclasses [NS], [AS], and [AH] (van Smeden, Janssens, Gooris, et al., 2014)	↓ very long CERs [EO] (van Smeden, Janssens, Boiten, et al., 2014)

Note Taken and modified from Bouwstra et al., (2021).

2.4. Molecular dynamics simulations

Molecular dynamics (MD) is a simulation technique in which Newtonian mechanics is used to calculate the evolution of a molecular system, which is dictated by the interaction forces between molecules. The force F_i acting on each atom caused by the surrounding atoms is calculated from the interaction potential, which is then used to determine the positions of the atoms over a short period of time, integrating Newton's second law of motion:

$$F_i = m_i . a_i \tag{2.1}$$

m_i is the mass of the atom, it $a_i = \frac{d^2 r_i}{dt^2}$ is acceleration and F_i the force acting on the atom.

As the force on each atom depends on the positions of the other atoms, a numerical integration algorithm is required. This time stepping process is repeated to produce a molecular trajectory comprising a time period (Rapaport, 2003).

2.4.1. Finite-difference methods

The standard approach for the numerical integration of the Newton's equations of motion is then the use of finite-difference methods, in which the integration over the time t is broken into a series of short time steps δt. At each time step, the forces $F_i(t)$ experienced by the particles in their current positions $r_i(t)$ are computed. It is then assumed that the $F_i(t)$ remain constant during the small-time step δt so that they can be combined with known dynamic information, position, velocities etc., at t, or preceding timesteps, to predict new positions etc. at the next time step $t + \delta t$. For this purpose, the finite-difference methods generally make use of truncated Taylor expansions for the position $r(t)$ and its derivatives, i.e., the velocity as first derivative, the acceleration as second derivative etc. (Eaker, 2018).

$$r_i(t+\delta t) = r_i(t) + v_i(t)\delta t + \frac{1}{2}a_i(t)\delta t^2 + \frac{1}{6}b_i(t)\delta t^3 + O(\delta t^4) \tag{2.2}$$

$$v_i(t+\delta t) = v_i(t) + a_i(t)\delta t + \frac{1}{2}b_i(t)\delta t^2 + O(\delta t^3) \tag{2.3}$$

$$a_i(t+\delta t) = a_i(t) + b_i(t)\delta t + O(\delta t^2) \tag{2.4}$$

$$b_i(t+\delta t) = b_i(t) + O(\delta t). \tag{2.5}$$

$O(\delta t^N)$ defines the order of the truncation error of the Taylor expansion.

2.4.1.1. Velocity Verlet. The Velocity Verlet algorithm is probably the most widely used finite-difference method today. The positions are derived from a Taylor expansion accurate to $\boldsymbol{O(\delta t^3)}$, whereas the velocity function only involves a Taylor expansion with $\boldsymbol{O(\delta t^2)}$. Though the velocities are forwarded in two stages that again involve a mid-step $\boldsymbol{\left(t+\frac{1}{2}\delta t\right)}$.

$$r_i(t+\delta t) = r_i(t) + v_i(t)\delta t + \frac{1}{2}a_i(t)\delta t^2 + O(\delta t^3) \tag{2.6}$$

$$v_i\left(t+\frac{1}{2}\delta t\right) = v_i(t) + a_i(t)\delta t + O(\delta t^2) \tag{2.7}$$

$$v_i\left(t+\frac{1}{2}\delta t\right) + a_i(t)\delta t + O(\delta t^2). \tag{2.8}$$

The positions $r_i(t+\delta t)$ are estimated from the current positions $r_i(t)$, velocities and accelerations. The current values $v_i(t)$ and $a_i(t)$ then also yield the velocities at the mid-step $v\left(t+\frac{1}{2}\delta t\right)$ as illustrated in Figure 3. For the new positions $r_i(t+\delta t)$, the forces are evaluated, which are then used together with the velocity at the mid-step $v_i\left(t+\frac{1}{2}\delta t\right)+a_i$ to calculate the velocity $v_i(t+\delta t)$. Then, both positions and velocities are available at $t+\delta t$, so that also the configurational energy and kinetic energy can be derived at the same timestep (Eaker, 2018; Raabe, 2017).

Figure 3

Illustration of the Velocity Verlet algorithm.

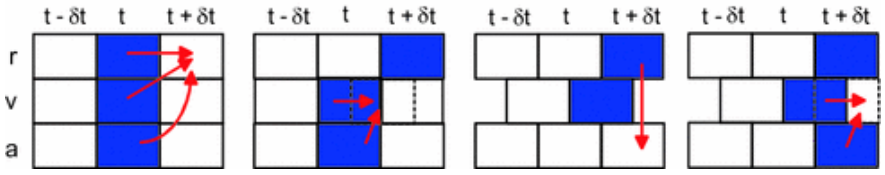

Note Taken and modified from Eaker (2018).

2.4.2. Thermostats in NVT ensemble and Barostats in NpT ensemble

Solving the Newton's equation of motion results in simulations in the NVE ensemble. However, this does not correspond to the conditions at which experimental studies are conducted. To derive thermophysical properties from MD simulations that can be compared with experimental data, it is necessary to perform simulations at constant temperature and/or constant pressure. To perform constant temperature simulations, so-called "thermostats" are used (Raabe, 2017).

The Maxwell-Boltzmann relation, equation 2.9, gives the probability distribution of the velocities of the particles of a system as a function of temperature and directly relates the kinetic energy of a system to its temperature. Solving the equation for the instantaneous temperature T

$$T(t) = \frac{\sum_{i=1}^{N} \frac{m_i}{2} . {v_i}^2}{N_f k_B} \tag{2.9}$$

where N_f represents the degrees of freedom of the system. This comprises the translational motion of the N particles in all three directions. Therefore, to control the temperature is to scale the velocities by a factor λ such that the resulting kinetic energy of the system corresponds to the imposed temperature T

$$T = \frac{\sum_{i=1}^{N} \frac{m_i}{2} . (\lambda\,(\mathrm{t}) v_i(t))^2}{N_f k_B} \tag{2.10}$$

Hence, the required scaling factor is given by

$$\lambda\,(\mathrm{t}) = \sqrt{\frac{T}{T(t)}} \tag{2.11}$$

The Berendsen thermostat (Berendsen et al., 1984) employs a time scale τ_T, so the scaling factor λ to update the velocity is given by

$$\lambda^2 = 1 + \frac{\delta t}{\tau_T}\left(\frac{T}{T(t)} - 1\right) \tag{2.12}$$

However, the Berendsen thermostat does not generate a canonical distribution of configurations (Hünenberger, 2015). There are more sophisticated approaches to control the temperature involve interactions of the system particles with a heat bath: as in a deterministic and dynamical approach as in the case of Nosé -Hoover thermostat (Hoover, 1985; Nosé, 1984).

Experimental studies usually are performed under condition of constant pressure. So, MD studies at conditions relevant for experiments require simulations not only to be performed at an imposed temperature, but often also at constant pressure. A macroscopic system reacts on an imposed pressure p by changing its volume. Accordingly, pressure control in simulation studies involves volume fluctuations of the simulation box. Therefore, the simplest approach to control the pressure is to scale the simulation volume (Uline & Corti, 2013). The counterpart to the Berendsen thermostat is the Berendsen barostat, which uses a scaling factor χ for the volume given by

$$\chi\,(t) = 1 - k_T\,\frac{\delta t}{\tau_p}\,(p - \wp) \tag{2.13}$$

τ_p is the time scale of the volume scaling, $\wp$ is the instantaneous pressure of the system, and k_T is the isothermal compressibility. The volume of the simulation box is then scaled by χ, whereas the center-of-mass coordinates of the particles and the cell factors are scaled by $\chi^{1/3}$.

2.4.3. Force Fields for MD simulation

The interaction between atoms or groups of atoms can be described at the quantum mechanical level or using molecular mechanics. The molecular mechanics approach is an approach in which the integrity of the molecule is generally maintained, i.e., there is no change in the covalent bond. The molecular structure is characterized by a "ball and spring" model, with the atoms being considered as spheres and linked together by springs. The potential energy of a molecular system and the associated intermolecular forces are calculated from a potential energy function, commonly referred to as a force field (Leach & AR, 2001), which describes the interaction potential as a function of a set of parameters. The potential energy function comprises bonding and non-bonding interactions (Figure 4). The bonding interactions refer to the contributions of bond stretching, angle bending and torsional rotation on bonds. Non-bonding interactions are assumed to act between atoms and comprise a van der Waals term, usually a Lennard-Jones potential, and a coulombic term to capture the electrostatic interaction between charged or partially charged atoms. The potential energy parameters that define the force field are input data in the simulations (Notman & Anwar, 2013). They are derived from a variety of sources that may include molecular beam experiments, spectroscopy and/or quantum mechanical calculations, which are optimized to reproduce experimental data. Force fields commonly employed for lipid simulations include AMBER (Cornell et al., 1995), GROMOS (Oostenbrink et al., 2004) and CHARMM (Brooks et al., 2009).

Figure 4

Potential energy function for molecular interactions in the molecular mechanics approximation. The first and second terms describe the van der Waals and coulombic interactions, respectively for atoms i and j. The next set of terms describes the bond, bond angle and torsional energy of the molecules composing the system. For the bond terms (bonds, bond angles and torsions), the potential energy is relative to the atoms that are in their equilibrium state, for which the energy is zero. The Lennard Jones parameters ε_{ij} and σ_{ij}, the partial charges q_i and q_j, and the force constants k_b, k_a, and k_ϕ are all atom-specific parameters that are introduced into the simulation.

$$U = \sum_{i<j} \sum 4\varepsilon_{ij}\left[\left(\frac{\sigma_{ij}}{r_{ij}}\right)^{12} - \left(\frac{\sigma_{ij}}{r_{ij}}\right)^{6}\right] + \sum_{i<j} \sum \frac{q_i q_j}{4\pi\varepsilon_0 r_{ij}} + \sum_{bonds} \frac{1}{2} k_b (r - r_0)^2 + \sum_{angles} \frac{1}{2} k_a (\theta - \theta_0)^2 + \sum_{torsions} k_\phi [1 + \cos(n\phi - \delta)]$$

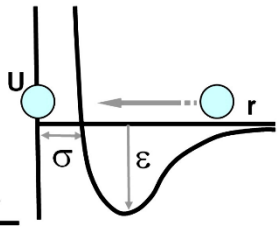

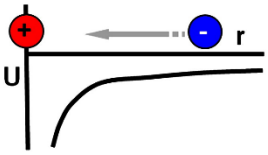

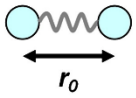

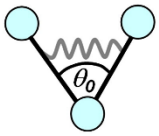

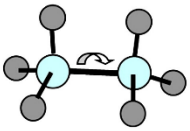

Note Taken from Notman and Anwar (2013).

2.4.4. Sampling techniques in molecular dynamics simulations of biological systems

Despite the success of MD simulations in studying a wide range of biological systems, they remain limited in two respects, inaccuracy of force fields and high computational cost, as reliable results are those obtained through simulations long enough for systems to sample all conformations (Bernardi et al., 2015). These limitations can result in inadequate sampling of conformational states, which in turn limits the ability to analyze and reveal the functional properties of the systems under examination.

To solve the problem of insufficient sampling, many improved sampling approaches have been developed. These methods are divided into two classes, depending on the definition of collective variables of the system. A collective variable is a function of atomic coordinates that can describe a certain motion or transition of interest. For example, the distance between two atoms

is a collective variable that can be used to describe bond formation and bond breaking, while a dihedral angle is often used to characterize an isomerization process (Liao, 2020).

The most used collective variable-based sampling methods are umbrella sampling (US) (Torrie & Valleau, 1977), metadynamics (MetaD) (Laio & Parrinello, 2002), directed molecular dynamics (SMD) (Lu & Schulten, 1999) temperature accelerated molecular dynamics (TAMD) (Maragliano & Vanden-Eijnden, 2006), among others. However, in some cases the selection of suitable collective variables to describe a system is not trivial, in these cases, sampling methods that do not use them are advantageous, since they allow sampling configurations without the need to know the system a priori. Within these sampling methods are replicate exchange (RE) (Sugita & Okamoto, 1999) and random walk (RWMD) (Moore et al., 2018).

Moore et al., (2018) developed and validated the RWMD equilibrium protocol, in which the simulation performs a random walk through a temperature space, allowing the system to exit metastable configurations and thus decouple from its initial configuration. The goal of the algorithm is that as the temperature increases, the free energy barriers are reduced, allowing different local minima to be explored each time the system returns from a high temperature to the lower temperature of interest. In this algorithm, the temperature of the system is adjusted in small time intervals, specifically, the sequence is defined within an interval between T_{min} and T_{max}, with discrete temperatures defined every ΔT.

To test the efficiency of RWMD Moore et al., (2018) used four models composed of CER[NS] and CHOL in equimolar mixtures with different initial configurations: the fully separated and coarse-grained checkerboard morphologies (Figure 5, a and b) serve as ‘‘bad’’ initial configurations, and the randomly mixed and fine-grained checkerboard systems (Figure 5, c and d) serve as reasonable, guesses of how to initialize mixed-lipid bilayers. Each initial morphology

was equilibrated for 200 ns with two different schemes: standard MD at 305 K, and RWMD with 305 K < T < 355 K. Through visual inspection, they compared the in-plane morphologies, and hence the equilibrium, of the different systems and equilibration procedures. At 305 K, the final morphologies visually resemble the corresponding initial morphologies. With RWMD, the final distributions of the lipids are visually distinct from the initial configuration, demonstrating that the lipids were able to reorganize. In the two most separated systems, the larger CHOL aggregates mostly break into smaller aggregates. Since each of these systems started from qualitatively different initial configurations, this result shows that the final configurations are de-correlated from the initial configurations.

Figure 5

System configurations. The first column shows the different initial configurations: (a) maximum phase separation; (b) Coarse-grained checkerboard; (c) randomly mixed; and (d) Fine-grained checkerboard. The second column shows the systems after 200 ns of MD at 305 K (e–h), the third column shows the systems after 200 ns of RWMD (i–l), and the fourth column shows the evolution of the CHOL-CHOL CN for each initial configuration (m–p). Snapshots are taken along the z axis, i.e., along the bilayer normal direction. eCER is represented as blue spheres and CHOL as yellow spheres.

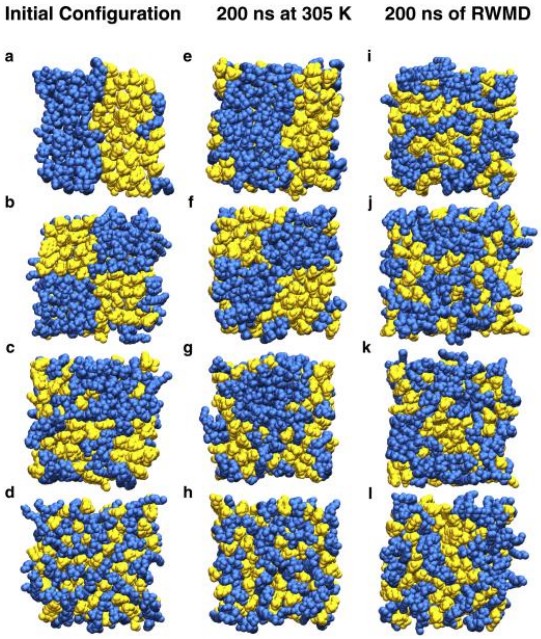

Note Taken from Moore et al., (2018).

3. Methodology

3.1. Obtaining the models of three stacked lipid bilayers

3.1.1. Models

Two models of three stacked lipid bilayers (Figure 6) were assembled using PACKMOL software (Martínez et al., 2009) with the following molar ratios:

- Composition CER[NP]:CER[AP] 1:2: CER[NP]:CER[AP]:CHOL:LA 0.66/0.34/0.7/1.
- Composition CER[NP]:CER[AP] 2:1: CER[NP]:CER[AP]:CHOL:LA 0.34/0.66/0.7/1.

To satisfy the defined molar ratios, each of the bilayers composing the models consists of 178 lipid molecules distributed as follows: 46 molecules of CHOL, 66 molecules of LA, 22 or 44 molecules of CER[NP] and 22 or 44 molecules of CER[AP] according to the required ratio. The models were hydrated with explicit solvent using the TIP3P water model (Jorgensen et al., 1983) with 4656 water molecules, 2150 water molecules on each outer surface and 178 water molecules with a lipid: water ratio of 1:2 in the monolayers forming the middle bilayer. The fully atomistic CHARMM36 force field (Klauda et al., 2010) supplemented by the CHARMM-compatible CER headgroup parameters from Guo et al. was used to describe CER[NP] (Guo et al., 2013) and Wang and Klauda for CER[AP] (Wang & Klauda, 2017).

Figure 6

a) *Front view (z-axis direction) of the CER[NP]:CER[AP] 1:2 stacked three-bilayer model after equilibration. Water is shown in gray, CER[NP] in pink, CER[AP] in green, LA in white and CHOL in light blue. The image was produced using VMD software* (Humphrey et al., 1996). ***b)*** *Structures of the lipids used. The CERs used consist of an 18-carbon phytosphingosine base attached to a 24-carbon saturated chain of a fatty acid (FA). Two ceramides were used that differ in the FA chain: CER[NP], which has a non-hydroxylated FA, and CER[AP], which has a hydroxylated FA.*

a)

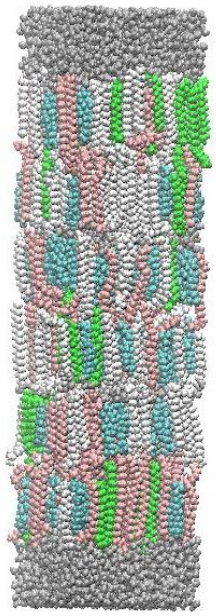

b)

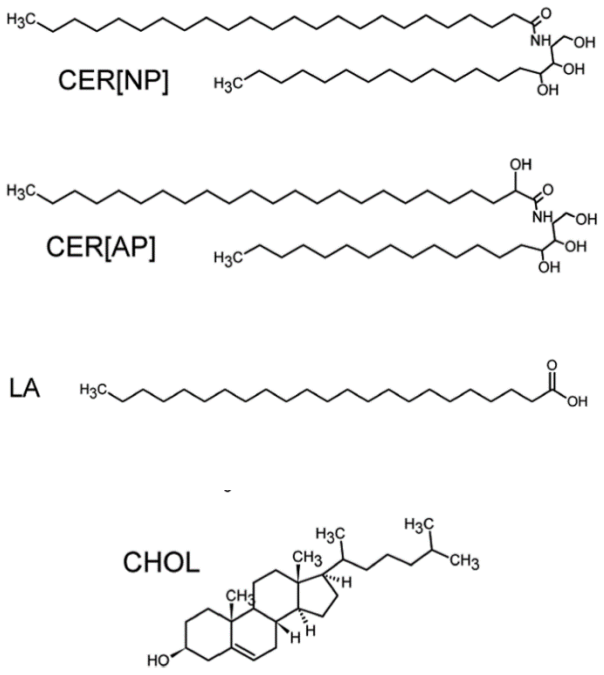

3.1.2. Packmol usage

To obtain the models with the Packmol software, it was necessary to provide an input file as shown in Appendix A. In this file the packing coordinates of each type of molecule were defined in regions of space whose shapes are defined by geometrical constraints. In lines 1 to 3, general aspects of the system are defined: the type of input file provided for each structure, the minimum distance between atoms of different molecules in Å and the name of the output file. Then, in the following lines, the number of molecules of each type to be placed inside a cube with specified minimum and maximum coordinates is defined. First, (0. 0. 0.) and (60. 60. 26.) were used as the minimum and maximum coordinates of the first monolayer, respectively, then 26 Å, a little more than that length of the CERs, were added in the z-coordinate for each monolayer. Furthermore, certain atoms are restricted to be above or below a plane to ensure the structure of a bilayer, in

which the polar groups interact with the aqueous medium and the hydrocarbon chains, i.e., the apolar part, interact with each other.

3.2. Molecular dynamics simulations

To eliminate energetically unfavorable contacts generated between the molecules during the construction of the models, energy minimization was carried out using the steepest descent method (van der Spoel et al., 2006) for each model for 5000 steps, until a potential energy gradient value $\Delta E \leq 1000$ kJ mol^{-1} nm^{-1} was reached.

Then, the oxygen atom in the head region of each lipid, as well as the dihedral angles in the acyl chains of CER[NP], CER[AP], LA and CHOL were harmonically constrained with a force constant of 1000 kJ mol^{-1} nm^{-2}, assigning initial velocities from a Maxwell-Boltzmann random distribution of 303.15 K. Thus, the model was balanced in six steps during which each constraint was uniformly relaxed to zero using the GROMACS 2021 simulation package (Lindahl et al., 2021). During equilibration, the three stacked lipid bilayers and the solvent were separately coupled in a heat bath using the Berendsen thermostat (Berendsen et al., 1984) with a relaxation constant τ_T = 1 ps. In the first two equilibration steps the models were simulated in an NVT assembly. Subsequently, steps three to six, these models were coupled to an NPT assembly using the Berendsen barostat (Berendsen et al., 1984) with a relaxation constant of τ_P = 5 ps and a semi-isotropic pressure coupling with a compressibility value of 4.5 $x10^{-5}$ bar^{-1}.

To reduce the effect of the initial structure of the molecules in the proposed models on the final molecular dynamics results the models were further simulated using the RWMD algorithm (Moore et al., 2018).

3.2.1. RWMD

In the RWMD algorithm, the temperature of the system is adjusted in small time intervals, so that the system performs a random walk through a temperature space. Specifically, the sequence is defined within an interval between T_{min} and T_{max}, with discrete temperatures defined every ΔT. In this work, the RWMD was performed for 150 ns, with temperature changes $\Delta T = 5xj(j\epsilon\{-1,0,1\})K$ every 5 ps, T_{min} = 303.15 K and T_{max} = 353.15 K for the first 75 ns and linearly reduced to 303.15 K for the last 75 ns. To avoid modification of the simulation code itself, we note that this random walk was determined separately, and the sequence of temperatures provided to the thermostat. A representative plot of the temperature versus time during the RWMD equilibrium is shown in Figure 7, where we note, the sequence defined in such a way as to sample all temperature states equally.

Figure 7

Representative plot of temperature versus time during the RWMD simulation.

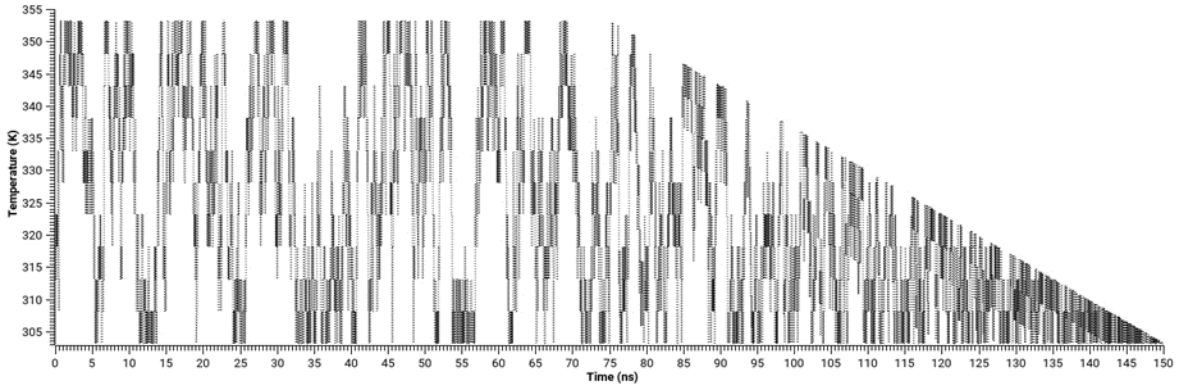

3.2.2. Production simulations

Production simulations were performed by generating 500 ns trajectories with an integration step of 2 fs. Temperature and pressure were controlled by the Nose Hover thermostat (Hoover, 1985; Nosé, 1984) and the Parrinello -Rahman barostat (Parrinello & Rahman, 1981),

respectively, maintaining the relaxation constants used in the equilibration. Electrostatic interactions were controlled using the Particle Mesh Ewald method (Essmann et al., 1995), applying a cutoff radius of 1.2 nm for the calculation of Coulombic and van der Waals interactions. Hydrogen bond lengths were constrained using the LINCS algorithm (Hess et al., 1997).

3.3. Analysis of results

The structural properties of the stratum corneum lipid matrix models were calculated over the 500 ns simulation at 303.15 K. To analyze the structure of the stacked three-layer models, several properties were calculated, including the thickness of the bilayers, the density profiles of various groups along the z-axis, the tilt angle of the lipid tails with respect to the z-axis, the distance between the terminal CH_3 and the top hydroxyl group, as explained in Appendix B, and the hydrogen bonds between the molecules and their orientations were investigated in detail. The results were compared with available experimental results (Schmitt, Lange, et al., 2018) and with the results obtained in our previous studies (Rivero, 2019).

Table 2 shows a summary of the procedure for calculating the structural properties mentioned above.

Table 2

Explanation of how the structural properties were calculated

Structural properties	Program/Tool	Procedure summary
Thickness	FATSLiM (Buchoux, 2017)	The polar head groups of each lipid were defined in an index. Each group represents the reference atoms for the upper and lower monolayer. FATSLiM considers one reference atom at a time, starting with the top monolayer, looking for the nearest neighbor to that reference point in the opposite monolayer in the x and y directions only. Then, the difference of the z-coordinates between the two reference atoms is the value representing the thickness in nanometers of the bilayer for each reference point. Thickness values were calculated every 0.02 ns.
Density profiles	GROMACS/ gmx density (Lindahl et al., 2021)	Several indexes were defined in these analyses:

Angle of the lipid tails	GROMACS/ gmx gangle (Lindahl et al., 2021)	- Including all atoms constituting each lipid type to calculate the density. - Including the initial and final carbons of the fatty acid chain, longest chain, of each CER. Forming a vector that allows the calculation of the angle between it and the positive z-plane.
Distance between specific groups	GROMACS/ gmx pairdist (Lindahl et al., 2021)	- Including the terminal CH_3 of the fatty acid chain of each CER in each monolayer and the 3- hydroxyl group (see Appendix B) to calculate the distance.
Hydrogen bonds	TRAVIS (Brehm et al., 2020; Brehm & Kirchner, 2011)	In this case, hydrogen bond donors and acceptors were determined, and inter- and intramolecular interactions were established. Estimation was performed through the distance and height of the first maximum in the X···H radial distribution function (RDF), together with the integral of the number up to the first minimum, to obtain the average number of hydrogen bonds of the X atom. Estimates of hydrogen bonds from pairwise RDFs were illustrated as a matrix of numbers (see Appendices I, J, and K). All analyses were performed on every tenth snapshot of MD.

4. Results

4.1. Effect of CERs composition on structural properties

4.1.1. General structural properties

Thickness is a necessary parameter to ensure that the assembled models represent the lipid extracellular matrix of the stratum corneum of the human epidermis. Table 3 shows the thickness calculated for each bilayer of each of the models. From the results it is possible to establish that both models, CER[NP]:CER[AP] 1:2 and 2:1, represent the stratum corneum lipid matrix because they hace a thickness in the range of 5.0 - 6.0 nm reported for the short periodicity phase (SPP) in native human stratum corneum (Das Chinmay & Olmsted Peter D., 2016; Elias, 2012).

Table 3

Thickness of the models of three stacked lipid bilayers.

Model	Thickness (nm)			
	Reported (Schmitt, Lange, et al., 2018)	Bottom bilayer (BB)	Middle bilayer (MB)	Upper bilayer (UB)
CER[NP]:CER[AP] 1:2	5.45 ± 0.1	5.49 ± 0.03	5.48± 0.03	5.49 ± 0.03
CER[NP]:CER[AP] 2:1		5.48 ± 0.04	5.44 ± 0.04	5.48 ± 0.04

The thickness values are within the value reported in the experimental study developed by Schmitt et al. (2018). With the better resolution offered by molecular dynamics simulations, it is possible to establish that the thickness of the bilayers decreases with increasing CER[NP] content, this effect being greater in the central bilayer. The location of each of the lipids was analyzed (Figure 8), especially in the contact zone between the monolayers, to determine whether there is overlap or contact between the acyl chains.

Figure 8

Profiles of total lipid mass density of the middle bilayer along the z axis, i.e., along the bilayer normal direction.

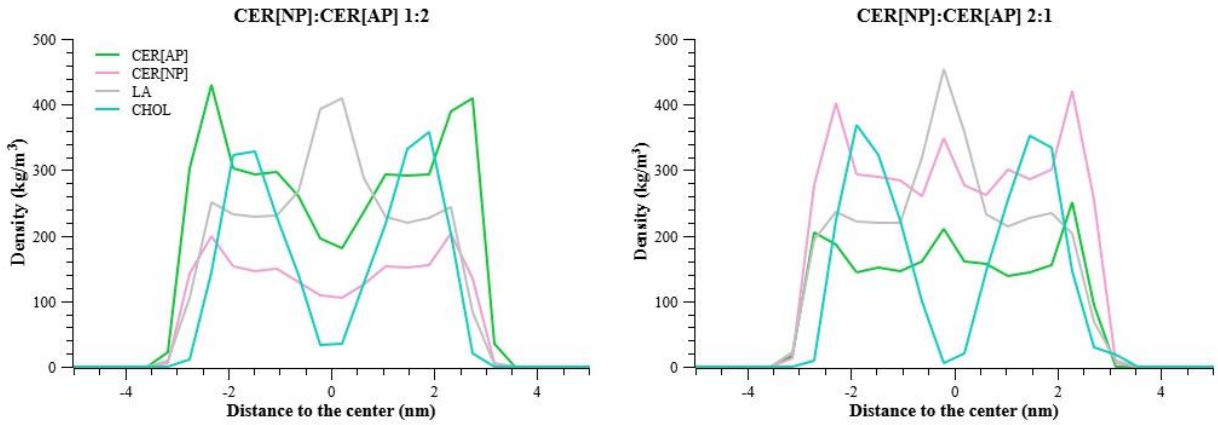

The models show mass density profiles containing the expected features of lipid bilayers. Near the lipid-water interface the profiles contain a peak which represents the heavy atoms of the lipid head groups in the upper and lower monolayer. Just after the headgroup region there is a high-density tail region where the tails are densely packed and highly ordered. In the center of each bilayer is a low-density tail region where the lipid tails are less densely packed and less ordered. This region exists mainly due to the asymmetry in tail lengths and is composed of the terminal part of the tails of the CERs and the LA. In the center of all profiles (see Appendix C) the LA has a very pronounced peak, indicating overlap between the acyl chains of one monolayer with the opposite monolayer. All profiles of the CER[NP]:CER[AP] 2:1 model, except CHOL, show

peaks in this same area, which may be due to possible contact between the acyl chains of each monolayer and not specifically to overlap, whereas in the CER[NP]:CER[AP] 1:2 model an opposite trend is observed for the CERs with a V-shape indicating a lower density.

To check whether the pronounced peak in the lipid density profile of the CER[NP]:CER[AP] 2:1 model indicates contact or overlap the distance between the 3-hydroxyl and the terminal CH_3 located in the same monolayer and the terminal CH_3 located in the opposite monolayer of CERs and LA was measured (as explained in Appendix B).

Figure 9

Histogram of the distance of the middle bilayer between the 3-hydroxyl and the terminal CH_3 of the fatty acid chain of CERs and chain LA of the same monolayer and of the opposite monolayer. See Appendixes D and E for the rest of bilayers.

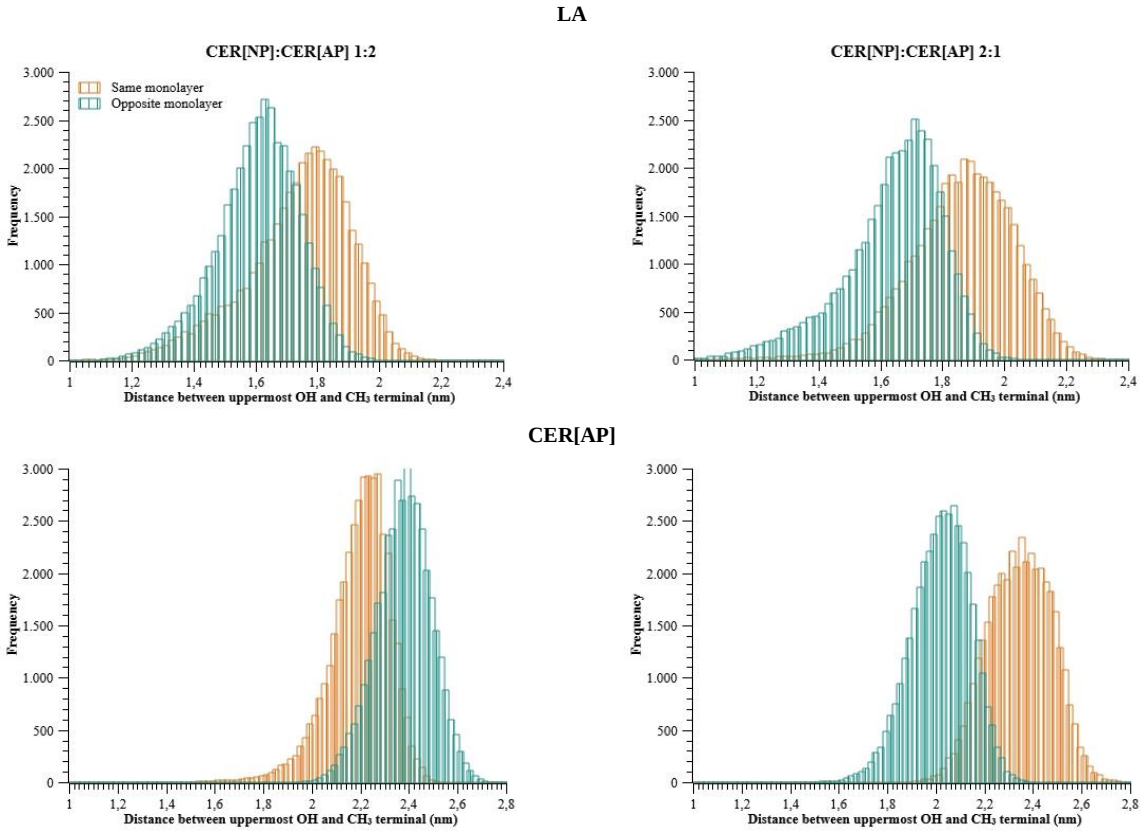

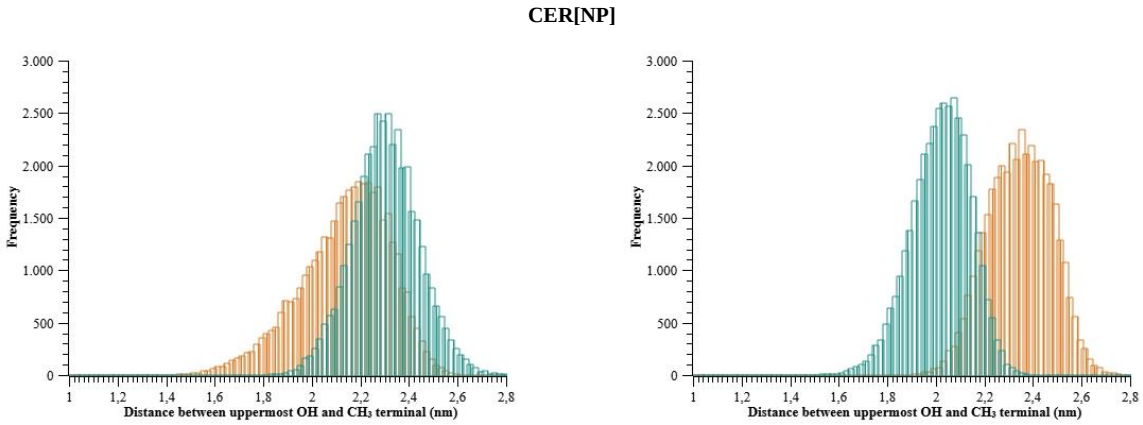

From these results it is possible to corroborate that the peaks appearing in the middle of the density profiles obtained in the CER[NP]:CER[AP] 2:1 model correspond to overlap because the distance between the 3-hydroxyl and the terminal CH_3 of the opposite monolayer is smaller than the distance between the same hydroxyl group and the terminal CH_3 of the same monolayer.

4.1.2. Angle of inclination

Figure 10 shows the histograms obtained for the angle of inclination calculated on the fatty acid chain of the CERs with respect to the z-axis, i.e., the axis perpendicular to the model of three stacked bilayers.

Figure 10

Histogram of the angle of inclination of the middle bilayer of the CER[NP], CER[AP] fatty acid chain and LA chain with respect to the z-axis. CER[NP]:CER[AP] 1:2 and CER[NP]:CER[AP] 2:1. See Appendix F for the rest of bilayers.

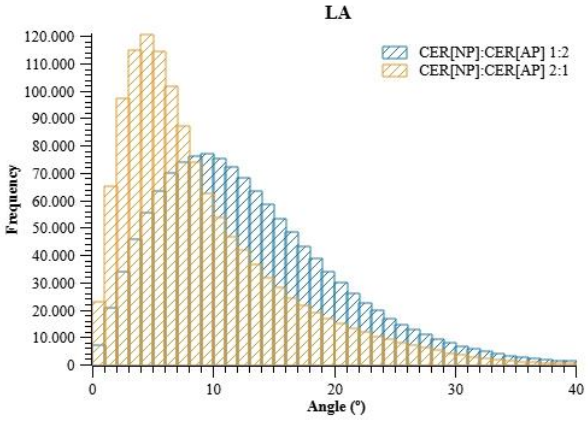

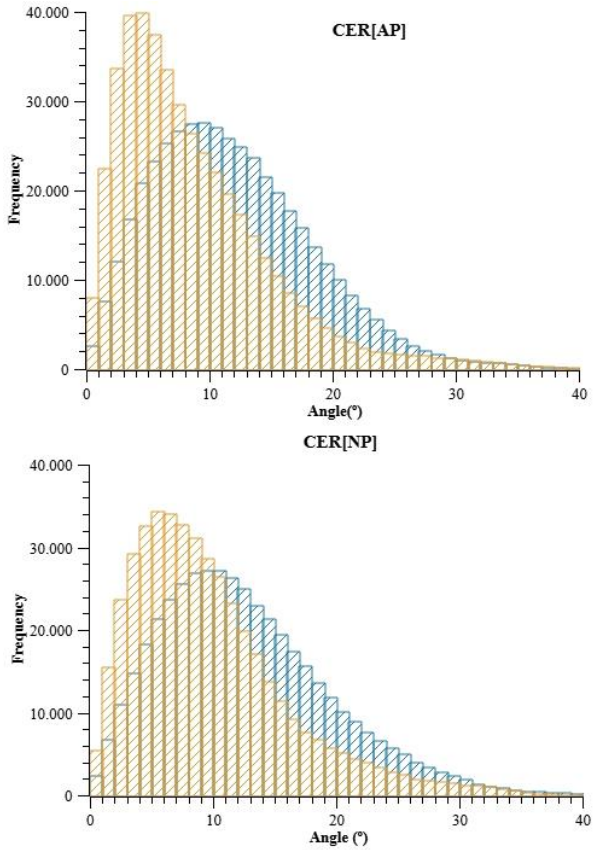

In the CER[NP]:CER[AP] 1:2 model the chains of both CERs and LA mainly present an angle of 10°. In the CER[NP]:CER[AP] 2:1 model CER[AP] and LA 4° and CER[NP] 6°. This indicates that there is some correlation with the Schmitt et al. results, however, from our results it is determined that in the 1:2 model the acyl chains are more inclined with respect to the acyl chains in the 2:1 model, i.e., they are not arranged in a completely straight conformation.

4.2. Hydrogen bonding

So far it has been possible to establish structural differences between the CER[NP]:CER[AP] 1:2 and 2:1 models, so there is a clear effect of the change in content of these CERs on the atomic-level structure of the stratum corneum lipid matrix, however, given that the only difference between CER[NP] and CER[AP] is an additional hydroxyl group in CER[AP] (Castro et al., 2014), and that it is not yet possible to find the cause of these dissimilarities, a

detailed analysis of the interactions, specifically of the formed hydrogen bonds, could provide an explanation. For this purpose, the number of hydrogen bonds formed between the CERs and each component (CERs, LA, CHOL and water) in the complete model, i.e., including all bilayers, and in the central bilayer including the two neighboring upper and lower monolayers were calculated.

Table 4

Total intermolecular interactions formed per CER molecule. Calculated in the complete models, i.e., in the three stacked bilayers, and only in the central bilayer including the neighboring monolayers.

Type	Number of hydrogen bonds formed per CER molecule			
	Whole model		Central bilayer with neighbor monolayers	
	CER[NP]:CER[AP] 1:2	CER[NP]:CER[AP] 2:1	CER[NP]:CER[AP] 1:2	CER[NP]:CER[AP] 2:1
CER[AP]-CER[AP]	1.84	1.55	2.01	1.67
CER[AP]-CER[NP]	0.50	0.90	0.60	1.00
CER[AP]-LA	0.70	0.60	0.90	0.70
CER[AP]-CHOL	0.30	0.30	0.40	0.30
CER[AP]-water	2.50	2.60	2.00	2.10
CER[AP]- any	**5.84**	**5.95**	**5.91**	**5.77**
CER[NP]-CER[AP]	1.00	0.40	1.20	0.50
CER[NP]-CER[NP]	0.60	1.40	0.80	1.60
CER[NP]-LA	0.70	0.50	0.70	0.60
CER[NP]-CHOL	0.20	0.20	0.20	0.20
CER[NP]-water	2.10	2.00	1.60	1.50
CER[NP]- any	**4.60**	**4.50**	**4.50**	**4.40**

It is important to note that the results in Table 4 show the same trend between the values obtained using the complete models and only the central bilayer with neighboring monolayers, however, as expected the values of hydrogen bonds formed with water decrease using the second method, since between the bilayers the number of water molecules added was much lower than that added on the outer surfaces.

The total number of hydrogen bonds formed by each CER is very similar in both ratios. The number of hydrogen bonds formed with LA, CHOL and water is not affected by the change in composition. However, it can be noted that the change in the composition of CERs modifies the interactions formed between these sphingolipids. The CER[AP] mainly forms hydrogen bonds with other CER[AP] and the number increases with the higher CER[AP] content. The same behavior is observed in CER[NP], however, this trend is not as strong because the number of bonds formed with CER[AP] is similar. Regardless of composition, CER[AP] forms more bonds with water than those formed by CER[NP]. Therefore, the adhesion of CER[AP] at the lipid-water interface is stronger.

To analyze in more detail, it is important to establish which of the total interactions of each type are intermolecular or intramolecular, as well as which acceptor and donor groups are involved. This information can be found in appendices I and J. Table 5 summarizes this information, specifically the most frequent intermolecular interactions between CERs that change with composition variation.

Table 5

Most common intermolecular interactions formed. All donor groups are listed with the most common acceptor group and in parentheses the number of hydrogen bonds formed between them per CER molecule. Calculated in the complete models, i.e., in the three stacked bilayers. Low in general represents values lower than 0.03. Appendix G shows all the results obtained in the complete model and J only in the central bilayer including the neighboring monolayers.

	Nomenclature
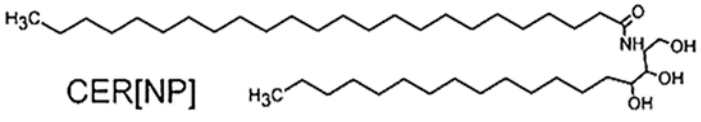 CER[NP]	Carbonyl Hydroxyl 3 Hydroxyl 2 Hydroxyl 1

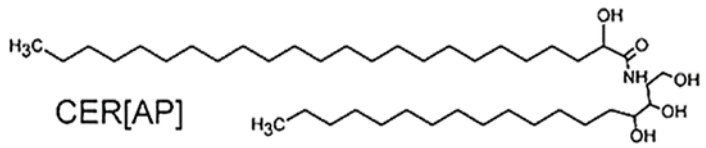

Acceptor		Donor			
		CER[AP]		CER[NP]	
		CER[NP]:CER[AP] 1:2	CER[NP]:CER[AP] 2:1	CER[NP]:CER[AP] 1:2	CER[NP]:CER[AP] 2:1
CER[AP]	O-Hydroxyl 1	H-N (0.10)	H-Hydroxyl 1 (0.17)	H-Hydroxyl 1 (0.06)	Low in general
	O-Hydroxyl 2	H-Hydroxyl 2 (0.10)	H-Hydroxyl 1 (0.15)	H-Hydroxyl 2 (0.06)	Low in general
	O-Hydroxyl 3	H-Hydroxyl 3 and Fatty Acid Hydroxyl (0.09)	H- Fatty Acid Hydroxyl (0.06)	H-Hydroxyl 3 (0.06)	Low in general
	H-N	Low in general	Low in general	Low in general	Low in general
	O-Carbonyl	H-N (0.13)	H-Hydroxyl 2 (0.10)	H-Hydroxyl 3 (0.09)	H-Hydroxyl 3 (0.05)
	O- Fatty Acid Hydroxyl	H-Hydroxyl 2, 3 and Fatty Acid Hydroxyl (0.08)	H-N (0.09)	H-Hydroxyl 3 (0.08)	Low in general
CER[NP]	O-Hydroxyl 1	Low in general	H-Hydroxyl 1 and 3 (0.04)	H-N (0.07)	H-N (0.14)
	O-Hydroxyl 2	H- Fatty Acid Hydroxyl (0.04)	H-Hydroxyl 1 (0.06)	Low in general	H-Hydroxyl 1 (0.10)
	O-Hydroxyl 3	Low in general	H-Hydroxyl 3 (0.09)	H-Hydroxyl 3 (0.07)	H-Hydroxyl 3 (0.11)
	H-N	Low in general	Low in general	Low in general	Low in general
	O-Carbonyl	H- Fatty Acid Hydroxyl (0.04)	H-N (0.09)	H-N (0.09)	H-N (0.15)
LA	O-Hydroxyl	H- Fatty Acid Hydroxyl (0.06)	H- Fatty Acid Hydroxyl (0.07)	H-Hydroxyl 1 (0.07)	Low in general
	O-Carbonyl	H-Hydroxyl 1 (0.16)	H- Fatty Acid Hydroxyl (0.11)	H-Hydroxyl 1 (0.23)	H-Hydroxyl 1 and (0.12) H-Hydroxyl 3 (0.15)
CHOL	O-Hydroxyl	H-Hydroxyl 3 (0.09)	H-N (0.07)	H-N (0.06)	H-Hydroxyl 1 (0.7)
Water	O	H-Hydroxyl 3 (0.56) and H- Fatty Acid Hydroxyl (0.91)	H-Hydroxyl 3 (0.87) and H- Fatty Acid Hydroxyl (0.60)	H-Hydroxyl 3 (0.90)	H-Hydroxyl 3 (0.90)

As general trends in both CERs it can be highlighted: the amide group as donor and acceptor establishes few interactions and water forms mainly hydrogen bonds with the O-Hydroxyl 3 and, also, in the case of CER[AP] with the oxygen of the fatty acid hydroxyl. In the behavior of the acceptor and donor groups of CER[AP] and CER[NP] no evident trends are observed, there is a high variability. It can be defined that in the CER[NP]:CER[AP] 1:2 model the hydroxyl groups 2 and 3 interact with these same groups of another CER[AP]. Furthermore, the hydrogen bonds formed with CER[NP] mainly form with the hydroxyl groups located at the same site, i.e., Hydroxyl 1 with Hydroxyl 1, Hydroxyl 2 with Hydroxyl 2, and Hydroxyl 3 with Hydroxyl 3.

In the case of intramolecular interactions (Table 6) the expected results are obtained, the number of hydrogen bonds formed of this type does not vary with the change in the composition of CERs, moreover, it is formed between consecutive donor and acceptor groups. The additional hydroxyl group forms less intramolecular interactions as an acceptor, however it is an donor of the carbonyl group, being this the most predominant interaction. In contrast, the CER[NP] that does not contain this additional group, the carbonyl interacts with Hydroxyl 3, being the interaction of this same group as a donor with Hydroxyl 2 the most prevalent.

Table 6

Specific intramolecular interactions formed per CER molecule. All major donor and acceptor groups are listed with the number of hydrogen bonds formed between them per CER molecule. Calculated in the complete models, i.e., in the three stacked bilayers. Low in general represents values less than 0.03. Appendix H shows all the results obtained in the complete model and J only in the central bilayer including the neighboring monolayers.

		Number of hydrogen bonds formed per CER molecule	
CER[AP]		**CER[NP]:CER[AP] 1:2**	**CER[NP]:CER[AP] 2:1**
Acceptor	**Donor**		
O-Hydroxyl 2	H-Hydroxyl 1	0.45	0.42
O-Hydroxyl 1	H-Hydroxyl 2	0.21	0.19
O-Hydroxyl 3	H-Hydroxyl 2	0.45	0.46
O-Carbonyl	H- Fatty Acid Hydroxyl	0.49	0.49
O- Fatty Acid Hydroxyl	H-N	0.05	0.05
N	H-Hydroxyl 3	0.13	0.10
CER[NP]			
O-Hydroxyl 2	H-Hydroxyl 1	0.27	0.34
O-Hydroxyl 1	H-Hydroxyl 2	0.22	0.22

O-Hydroxyl 3	H-Hydroxyl 2	0.43	0.46
O-Carbonyl	H-Hydroxyl 3	0.12	0.11
N	H-Hydroxyl 3	0.14	0.14

As it has been reported that CER[NS] exhibits interlayer hydrogen bonds, i.e., between the components of two adjacent monolayers that do not constitute the same bilayer, as a unique feature of this species of CER (Schmitt & Neubert, 2018). This type of interactions was calculated in CER[NP] and CER[AP] to determine whether the formation of this type of hydrogen bonds is possible. To obtain information on interlayer H-bonds three analyses were performed:

(1) central bilayer with neighboring monolayers (intra- and interlayer H-bonds are obtained).

(2) central bilayer only (intra-layer H-bonds in the central bilayer are obtained).

(3) only neighboring monolayers of the central bilayer (intra bilayer H-bonds are obtained in the two monolayers adjacent to the central bilayer).

The difference 1-2-3 results in the interlayer H-bonds, but it is necessary to consider that there are different numbers of molecules in 1,2 and 3. Therefore, the number of H-bonds is calculated from the average number of H-bonds per molecule, multiplied by the number of molecules:

$$\text{Interlayer Hb} = \frac{\text{number of Hbonds in (1)} - \text{number of Hbonds in (2)} - \text{number of Hbonds in (3}}{\text{number of CERs in (1)}} \quad (4.11)$$

From the results shown in Appendix I it is possible to establish the low occurrence of these interlayer interactions between the CERs under study, although their formation is not ruled out.

5. Results Discussion

5.1. Dependence of structural properties on ceramide composition

The results found in this study demonstrate that there is an effect on the structural properties of the stratum corneum lipid extracellular matrix caused by the change in the CER[NP]:CER[AP] ratio. Specifically, by varying between the native and diseased ratios, i.e., CER[NP]:CER[AP] 2:1 to 1:2, a higher angle of inclination of the acyl chains and an increased bilayer thickness were observed. In studies with molecular dynamics simulations performed by Antunes and Cavaco-Paulo (2020) it was reported for a model with higher CER[AP] concentration with respect to CER[NP], similar to the 1:2 composition of this study, an unusually stable and inclined packing, which promotes compactness, i.e., increased bilayer thickness was observed.

Figure 10 shows that the conformation of the lipid acyl chains in both models is mostly inclined as reported for orthorhombic lateral chain packing (Schmitt & Neubert, 2018). This finding is similar to that reported by Schmitt et al. However, it was established that in the CER[NP]:CER[AP] 2:1 model the acyl chains of the lipids are not completely straight. They have a minor tilt, although less than that of the lipid acyl chains in the CER[NP]:CER[AP]1:2 model.

There are no previous studies evaluating the total number of hydrogen bonds formed in models of similar content to those studied. Only one investigation evaluated a model containing only CER[AP] and showed almost no interlayer interactions (Gruzinov et al., 2017) consistent with our observations.

5.2. Improved results

From the results obtained, it was found that the use of a model of three stacked lipid bilayers, the simplest model representing the stratum corneum lipid matrix, because it ensures that one bilayer is in the middle of two more bilayers, better reproduces the results reported by Schmitt

et al (2018) (Figure 11) than the model of a single lipid bilayer (Rivero, 2019). To ensure this, it should be noted that this study used:

(1) the same isomer for CER[AP], N-(α-d-hydroxytetracosanoyl)-phytosphingosine (CER[AP]) and equal ratios of CER[NP]:CER[AP]:LA:CHOL:water employed in the experimental study.

(2) a force field supplemented with CHARMM-compatible CER headgroup parameters from Guo et al. was used to describe CER[NP] and Wang and Klauda for CER[AP].

(3) an improved sampling protocol to ensure that the results of molecular dynamics simulations do not depend on the initial modeling arrangements.

Figure 11

Proposed arrangement by Schmitt et al for CER[NP]:[AP] 2:1 and 1:2 ratio models including CHOL and LA.

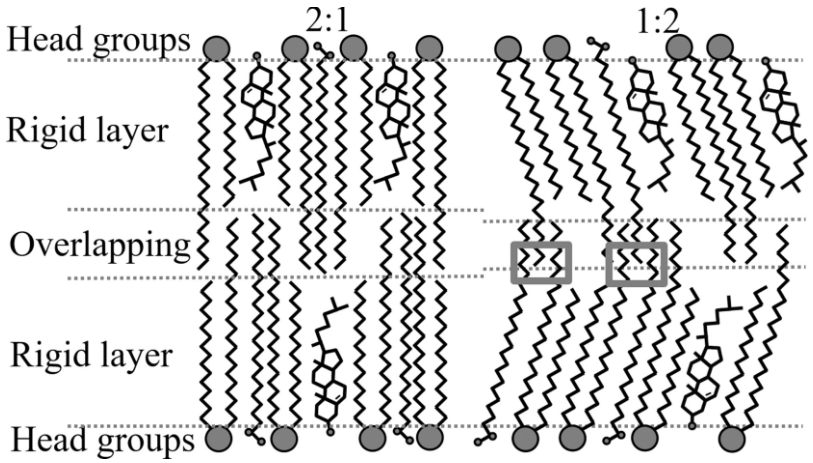

Note Taken from Schmitt et al. (2018).

As can be seen in Figure 12, when using a single bilayer model, no differences in the tilt angles between the CER[NP]:CER[AP] 1:2 and 2:1 ratio are evident. Likewise, no overlap was determined in either case and the thickness (5.11 ± 0.62 for CER[NP]:CER[AP] 1:2 and 5.00 ± 0.42 for CER[NP]:CER[AP] 2:1) reported is within a larger range due to less successful equilibration of the models. This may be caused by the fact that in the stratum corneum lipid matrix

the great majority of bilayers are in contact with one upper and one lower bilayer (Elias, 2012), generating a repetitive pattern, therefore, this model does not represent these characteristics.

Figure 12

Histogram of the angle of inclination of the CER[NP], CER[AP] fatty acid chain and LA chain with respect to the z-axis. CER[NP]:CER[AP] 1:2 and CER[NP]:CER[AP] 2:1) calculated in a bilayer model (Rivero, 2019).

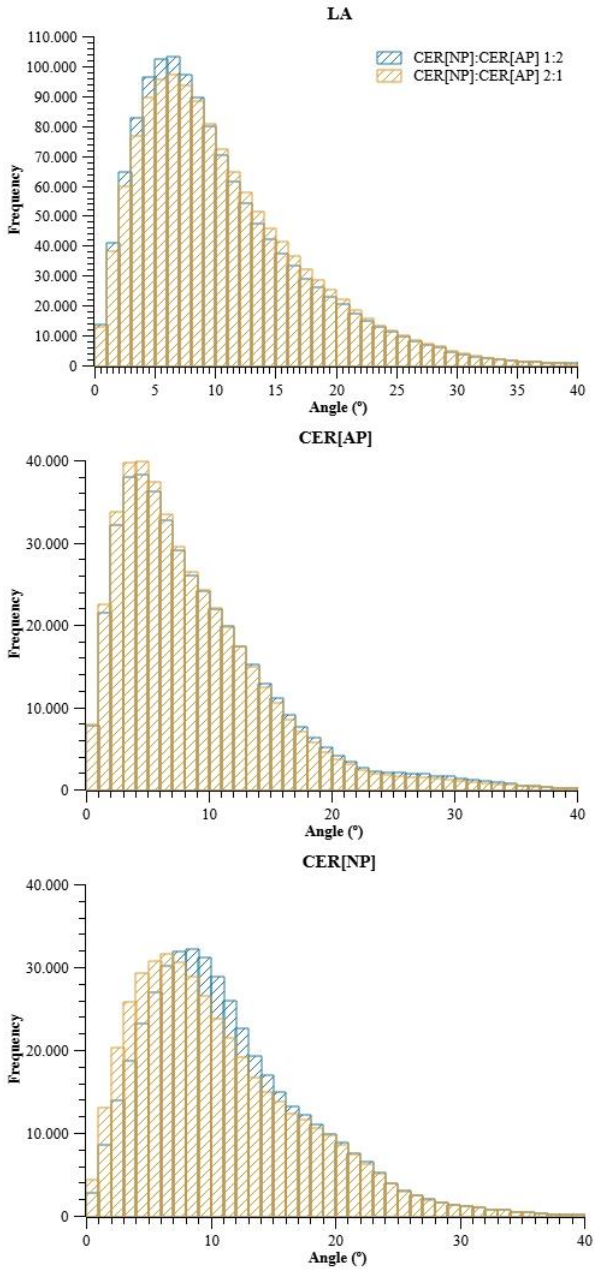

Note Taken from Rivero (2019).

6. Conclusions

In this study using molecular dynamics simulations it was determined that the change in CERs composition affects the structural properties of the stratum corneum lipid matrix. A higher CER[AP] content induces a lower bilayer thickness, a higher tilt angle of the acyl chains and the terminal CH_3 of the acyl chains of one monolayer only contact and do not overlap with those of the opposite monolayer.

The observed trends for the hydrogen bonds between CER molecules are consistent with the composition. For example, in the simulations with more CER[AP], more hydrogen bonds are formed with CER[AP] and with its higher number of H-bond donors, CER[AP] forms more hydrogen bonds. A more detailed analysis shows that in CER[AP] and CER[NP] the 3-OH group forms more H-bonds than the other donors.

CER[AP] forms more H-bonds than CER[NP], consistent with its larger number of H-bond donors, Many of these H-bonds are with water, but also without including H-bonds with water in the analysis, the same trend is found. In general, the total number of intermolecular hydrogen bonds formed by each CER is the same in both ratios.

With the results obtained, it was confirmed that the use of a more representative model of the stratum corneum lipid matrix with three stacked lipid bilayers improves the results of the molecular dynamics simulations because it reproduces the reported experimental results and interpretations and allows identifying the differences between the bilayers that are in contact with other bilayers and the bilayers of the external surfaces that present more contact with the solvent.

7. Future Works

- To evaluate the effect of the addition of other compounds on the structure of the stratum corneum lipid matrix model.

- To evaluate the effect of the addition of other CERs on the structural properties of the stratum corneum lipid matrix model and their influence on the formation of long periodicity phases (LPP). For example, CERs with longer fatty acid chain length, such as CER[EOS].

- To study the effect of L- and D-isomers of CER[NP] and CER[AP] on the structure of the stratum corneum lipid matrix model.

8. Results Communications

- Oral Presentation: "Effect of the CER[NP]:CER[AP] composition on the structural properties of a model the lipid matrix of the stratum corneum of the human epidermis". Natalia Rivero, Markus Doerr, Martha C. Daza. 2nd Conference of Women in Bioinformatics and Data Science LA. September 2021.

- Oral Presentation: "Dinámica molecular de un modelo de bicapa lipídica del estrato córneo de la epidermis humana". Natalia Rivero, Markus Doerr, Martha C. Daza. Encuentro Modelamiento Molecular Colombia 2020. December 2020.

- Poster: "Effect of the Ceramide Composition on the Structure of a Stratum Corneum Model System". Natalia Rivero, Markus Doerr, Martha C. Daza. 1st Congress of Women in Bioinformatics and Data Science Latin America. September 2020.

- Poster: "Molecular Dynamics Simulation of a CER[NP]-and [AP]-Based Stratum Corneum Model". Natalia Rivero, Markus Doerr, Martha C. Daza. LatinXChem Twitter Conference 2020. August 2020.

Bibliographic References

Agrawal, K., Hassoun, L. A., Foolad, N., Borkowski, K., Pedersen, T. L., Sivamani, R. K., & Newman, J. W. (2018). Effects of atopic dermatitis and gender on sebum lipid mediator and fatty acid profiles. *Prostaglandins, Leukotrienes, and Essential Fatty Acids*, *134*, 7–16. https://doi.org/10.1016/j.plefa.2018.05.001

Berendsen, H. J. C., Postma, J. P. M., van Gunsteren, W. F., DiNola, A., & Haak, J. R. (1984). Molecular dynamics with coupling to an external bath. *The Journal of Chemical Physics*, *81*(8), 3684–3690. https://doi.org/10.1063/1.448118

Bernardi, R. C., Melo, M. C. R., & Schulten, K. (2015). Enhanced sampling techniques in molecular dynamics simulations of biological systems. *Recent Developments of Molecular Dynamics*, *1850*(5), 872–877. https://doi.org/10.1016/j.bbagen.2014.10.019

Boncheva, M. (2012). Molecular Organization of the Lipid Matrix in Stratum Corneum and Its Relevance for the Protective Functions of Human Skin. In M. Lodén & H. I. Maibach (Eds.), *Treatment of Dry Skin Syndrome: The Art and Science of Moisturizers* (pp. 125–147). Springer. https://doi.org/10.1007/978-3-642-27606-4_10

Bouwstra, J. A., Dubbelaar, F. E., Gooris, G. S., & Ponec, M. (2000). The lipid organisation in the skin barrier. *Acta Dermato-Venereologica. Supplementum*, *208*, 23–30. https://doi.org/10.1080/000155500750042826

Bouwstra, J. A., Helder, R. W. J., & El Ghalbzouri, A. (2021). Human skin equivalents: Impaired barrier function in relation to the lipid and protein properties of the stratum corneum. *Advanced Drug Delivery Reviews*, *175*, 113802. https://doi.org/10.1016/j.addr.2021.05.012

Bouwstra, J. A., & Ponec, M. (2006). The skin barrier in healthy and diseased state. *Biochimica et Biophysica Acta (BBA) - Biomembranes*, *1758*(12), 2080–2095. https://doi.org/10.1016/j.bbamem.2006.06.021

Brehm, M., & Kirchner, B. (2011). TRAVIS - A Free Analyzer and Visualizer for Monte Carlo and Molecular Dynamics Trajectories. *Journal of Chemical Information and Modeling*, *51*(8), 2007–2023. https://doi.org/10.1021/ci200217w

Brehm, M., Thomas, M., Gehrke, S., & Kirchner, B. (2020). TRAVIS—A free analyzer for trajectories from molecular simulation. *The Journal of Chemical Physics*, *152*(16), 164105. https://doi.org/10.1063/5.0005078

Brooks, B. R., Brooks, C. L., MacKerell, A. D., Nilsson, L., Petrella, R. J., Roux, B., Won, Y., Archontis, G., Bartels, C., Boresch, S., Caflisch, A., Caves, L., Cui, Q., Dinner, A. R., Feig, M., Fischer, S., Gao, J., Hodoscek, M., Im, W., … Karplus, M. (2009). CHARMM: The Biomolecular Simulation Program. *Journal of Computational Chemistry*, *30*(10), 1545–1614. https://doi.org/10.1002/jcc.21287

Buchoux, S. (2017). FATSLiM: a fast and robust software to analyze MD simulations of membranes. *Bioinformatics*, *33*(1), 133–134. https://doi.org/10.1093/bioinformatics/btw563

Castro, B. M., Prieto, M., & Silva, L. C. (2014). Ceramide: A simple sphingolipid with unique biophysical properties. *Progress in Lipid Research*, *54*, 53–67. https://doi.org/10.1016/j.plipres.2014.01.004

Checa, A., Xu, N., Sar, D. G., Haeggström, J. Z., Ståhle, M., & Wheelock, C. E. (2015). Circulating levels of sphingosine-1-phosphate are elevated in severe, but not mild psoriasis and are

unresponsive to anti-TNF-α treatment. *Scientific Reports*, *5*, 12017. https://doi.org/10.1038/srep12017

Cornell, W. D., Cieplak, P., Bayly, C. I., Gould, I. R., Merz, K. M., Ferguson, D. M., Spellmeyer, D. C., Fox, T., Caldwell, J. W., & Kollman, P. A. (1995). A Second Generation Force Field for the Simulation of Proteins, Nucleic Acids, and Organic Molecules. *Journal of the American Chemical Society*, *117*(19), 5179–5197. https://doi.org/10.1021/ja00124a002

Das, C., Noro, M. G., & Olmsted, P. D. (2009). Simulation Studies of Stratum Corneum Lipid Mixtures. *Biophysical Journal*, *97*(7), 1941–1951. https://doi.org/10.1016/j.bpj.2009.06.054

Das Chinmay, & Olmsted Peter D. (2016). The physics of stratum corneum lipid membranes. *Philosophical Transactions of the Royal Society A: Mathematical, Physical and Engineering Sciences*, *374*(2072), 20150126. https://doi.org/10.1098/rsta.2015.0126

Eaker, C. W. (2018). Molecular Dynamics Simulations. In *Salem Press Encyclopedia of Science*. Salem Press.

Elias, P. M. (2005). Stratum Corneum Defensive Functions: An Integrated View. *Journal of Investigative Dermatology*, *125*(2), 183–200. https://doi.org/10.1111/j.0022-202X.2005.23668.x

Elias, P. M. (2012). Structure and Function of the Stratum Corneum Extracellular Matrix. *The Journal of Investigative Dermatology*, *132*(9), 2131–2133. https://doi.org/10.1038/jid.2012.246

Essmann, U., Perera, L., Berkowitz, M. L., Darden, T., Lee, H., & Pedersen, L. G. (1995). A smooth particle mesh Ewald method. *The Journal of Chemical Physics*, *103*(19), 8577–8593. https://doi.org/10.1063/1.470117

Goto-Inoue, N., Hayasaka, T., Zaima, N., Nakajima, K., Holleran, W. M., Sano, S., Uchida, Y., & Setou, M. (2012). Imaging mass spectrometry visualizes ceramides and the pathogenesis of dorfman-chanarin syndrome due to ceramide metabolic abnormality in the skin. *PloS One*, *7*(11), e49519. https://doi.org/10.1371/journal.pone.0049519

Gruzinov, A. Yu., Zabelin, A. V., & Kiselev, M. A. (2017). Short periodicity phase based on ceramide [AP] in the model lipid membranes of stratum corneum does not change during hydration. *Chemistry and Physics of Lipids*, *202*, 1–5. https://doi.org/10.1016/j.chemphyslip.2016.11.002

Guo, S., Moore, T. C., Iacovella, C. R., Strickland, L. A., & McCabe, C. (2013). Simulation study of the structure and phase behavior of ceramide bilayers and the role of lipid head group chemistry. *Journal of Chemical Theory and Computation*, *9*(11), 5116–5126. https://doi.org/10.1021/ct400431e

Gupta, R., Dwadasi, B. S., & Rai, B. (2016). Molecular Dynamics Simulation of Skin Lipids: Effect of Ceramide Chain Lengths on Bilayer Properties. *The Journal of Physical Chemistry. B*, *120*(49), 12536–12546. https://doi.org/10.1021/acs.jpcb.6b08059

Hess, B., Bekker, H., Berendsen, H. J. C., & Fraaije, J. G. E. M. (1997). LINCS: A linear constraint solver for molecular simulations. *Journal of Computational Chemistry*, *18*(12), 1463–1472. https://doi.org/10.1002/(SICI)1096-987X(199709)18:12<1463::AID-JCC4>3.0.CO;2-H

Hoover, W. G. (1985). Canonical dynamics: Equilibrium phase-space distributions. *Physical Review A*, *31*(3), 1695–1697. https://doi.org/10.1103/PhysRevA.31.1695

Humphrey, W., Dalke, A., & Schulten, K. (1996). VMD: visual molecular dynamics. *Journal of Molecular Graphics*, *14*(1), 33–38, 27–28.

Hünenberger, P. H. (2015). Thermostat Algorithms for Molecular Dynamics Simulations. *Advanced Computer Simulation*, 105–149. https://doi.org/10.1007/b99427

Imokawa, G., Abe, A., Jin, K., Higaki, Y., Kawashima, M., & Hidano, A. (1991). Decreased level of ceramides in stratum corneum of atopic dermatitis: an etiologic factor in atopic dry skin? *The Journal of Investigative Dermatology*, *96*(4), 523–526. https://doi.org/10.1111/1523-1747.ep12470233

Janssens, M., Gooris, G. S., & Bouwstra, J. A. (2009). Infrared spectroscopy studies of mixtures prepared with synthetic ceramides varying in head group architecture: Coexistence of liquid and crystalline phases. *Biochimica et Biophysica Acta (BBA) - Biomembranes*, *1788*(3), 732–742. https://doi.org/10.1016/j.bbamem.2009.01.003

Jorgensen, W. L., Chandrasekhar, J., Madura, J. D., Impey, R. W., & Klein, M. L. (1983). Comparison of simple potential functions for simulating liquid water. *The Journal of Chemical Physics*, *79*(2), 926–935. https://doi.org/10.1063/1.445869

Kashibuchi, N., Hirai, Y., O'Goshi, K., & Tagami, H. (2002). Three-dimensional analyses of individual corneocytes with atomic force microscope: morphological changes related to age, location and to the pathologic skin conditions. *Skin Research and Technology: Official Journal of International Society for Bioengineering and the Skin (ISBS) [and] International Society for Digital Imaging of Skin (ISDIS) [and] International Society for Skin Imaging (ISSI)*, *8*(4), 203–211. https://doi.org/10.1034/j.1600-0846.2002.00348.x

Klauda, J. B., Venable, R. M., Freites, J. A., O'Connor, J. W., Tobias, D. J., Mondragon-Ramirez, C., Vorobyov, I., MacKerell, A. D., & Pastor, R. W. (2010). Update of the CHARMM All-Atom Additive Force Field for Lipids: Validation on Six Lipid Types. *The Journal of Physical Chemistry B, 114*(23), 7830–7843. https://doi.org/10.1021/jp101759q

Laio, A., & Parrinello, M. (2002). Escaping free-energy minima. *Proceedings of the National Academy of Sciences of the United States of America*, *99*(20), 12562–12566. https://doi.org/10.1073/pnas.202427399

Lampe, M. A., Burlingame, A. L., Whitney, J., Williams, M. L., Brown, B. E., Roitman, E., & Elias, P. M. (1983). Human stratum corneum lipids: characterization and regional variations. *Journal of Lipid Research*, *24*(2), 120–130.

Lavrijsen, A. P. M., Bouwstra, J. A., Gooris, G. S., Weerheim, A., Boddé, H. E., & Ponec, M. (1995). Reduced Skin Barrier Function Parallels Abnormal Stratum Corneum Lipid Organization in Patients with Lamellar Ichthyosis. *Journal of Investigative Dermatology*, *105*(4), 619–624. https://doi.org/10.1111/1523-1747.ep12323752

Leach, A. R., & AR, L. (2001). *Molecular Modelling: Principles and Applications*. Prentice Hall.

Li, L., Tang, X., Taylor, K. G., DuPré, D. B., & Yappert, M. C. (2002). Conformational characterization of ceramides by nuclear magnetic resonance spectroscopy. *Biophysical Journal*, *82*(4), 2067–2080. https://www.ncbi.nlm.nih.gov/pmc/articles/PMC1302001/

Li, S., Ganguli-Indra, G., & Indra, A. K. (2016). Lipidomic analysis of epidermal lipids: a tool to predict progression of inflammatory skin disease in humans. *Expert Review of Proteomics*, *13*(5), 451–456. https://doi.org/10.1080/14789450.2016.1177462

Liao, Q. (2020). Enhanced sampling and free energy calculations for protein simulations. *Progress in Molecular Biology and Translational Science*, *170*, 177–213. https://doi.org/10.1016/bs.pmbts.2020.01.006

Lindahl, Abraham, Hess, & Spoel, van der. (2021). *GROMACS 2021 Manual*. https://doi.org/10.5281/zenodo.4457591

Lu, H., & Schulten, K. (1999). Steered molecular dynamics simulations of force-induced protein domain unfolding. *Proteins: Structure, Function, and Bioinformatics*, *35*(4), 453–463. https://doi.org/10.1002/(SICI)1097-0134(19990601)35:4<453::AID-PROT9>3.0.CO;2-M

Ludovici, M., Kozul, N., Materazzi, S., Risoluti, R., Picardo, M., & Camera, E. (2018). Influence of the sebaceous gland density on the stratum corneum lipidome. *Scientific Reports*, *8*(1), 11500. https://doi.org/10.1038/s41598-018-29742-7

Maragliano, L., & Vanden-Eijnden, E. (2006). A temperature accelerated method for sampling free energy and determining reaction pathways in rare events simulations. *Chemical Physics Letters*, *426*(1), 168–175. https://doi.org/10.1016/j.cplett.2006.05.062

Martínez, L., Andrade, R., Birgin, E. G., & Martínez, J. M. (2009). PACKMOL: a package for building initial configurations for molecular dynamics simulations. *Journal of Computational Chemistry*, *30*(13), 2157–2164. https://doi.org/10.1002/jcc.21224

Masukawa, Y., Narita, H., Shimizu, E., Kondo, N., Sugai, Y., Oba, T., Homma, R., Ishikawa, J., Takagi, Y., Kitahara, T., Takema, Y., & Kita, K. (2008). Characterization of overall ceramide species in human stratum corneum. *Journal of Lipid Research*, *49*(7), 1466–1476. https://doi.org/10.1194/jlr.M800014-JLR200

Matoltsy, A. G. (1976). Keratinization. *The Journal of Investigative Dermatology*, *67*(1), 20–25. https://doi.org/10.1111/1523-1747.ep12512473

Matsumoto, M., Umemoto, N., Sugiura, H., & Uehara, M. (1999). Difference in ceramide composition between “dry” and “normal” skin in patients with atopic dermatitis. *Acta Dermato-Venereologica*, *79*(3), 246–247. https://doi.org/10.1080/000155599750011183

Menon, G. K., Cleary, G. W., & Lane, M. E. (2012). The structure and function of the stratum corneum. *International Journal of Pharmaceutics*, *435*(1), 3–9. https://doi.org/10.1016/j.ijpharm.2012.06.005

Moore, T. C., Hartkamp, R., Iacovella, C. R., Bunge, A. L., & McCabe, C. (2018). Effect of Ceramide Tail Length on the Structure of Model Stratum Corneum Lipid Bilayers. *Biophysical Journal*, *114*(1), 113–125. https://doi.org/10.1016/j.bpj.2017.10.031

Motta, S., Monti, M., Sesana, S., Caputo, R., Carelli, S., & Ghidoni, R. (1993). Ceramide composition of the psoriatic scale. *Biochimica et Biophysica Acta (BBA) - Molecular Basis of Disease*, *1182*(2), 147–151. https://doi.org/10.1016/0925-4439(93)90135-N

Nosé, S. (1984). A molecular dynamics method for simulations in the canonical ensemble. *Molecular Physics*, *52*(2), 255–268. https://doi.org/10.1080/00268978400101201

Notman, R., & Anwar, J. (2013). Breaching the skin barrier--insights from molecular simulation of model membranes. *Advanced Drug Delivery Reviews*, *65*(2), 237–250. https://doi.org/10.1016/j.addr.2012.02.011

Oostenbrink, C., Villa, A., Mark, A. E., & van Gunsteren, W. F. (2004). A biomolecular force field based on the free enthalpy of hydration and solvation: the GROMOS force-field parameter sets 53A5 and 53A6. *Journal of Computational Chemistry*, *25*(13), 1656–1676. https://doi.org/10.1002/jcc.20090

Paige, D. G., Morse-Fisher, N., & Harper, J. I. (1994). Quantification of stratum corneum ceramides and lipid envelope ceramides in the hereditary ichthyoses. *The British Journal of Dermatology*, *131*(1), 23–27. https://doi.org/10.1111/j.1365-2133.1994.tb08452.x

Parrinello, M., & Rahman, A. (1981). Polymorphic transitions in single crystals: A new molecular dynamics method. *Journal of Applied Physics*, *52*(12), 7182–7190. https://doi.org/10.1063/1.328693

Pilgram, G. S., Vissers, D. C., van der Meulen, H., Pavel, S., Lavrijsen, S. P., Bouwstra, J. A., & Koerten, H. K. (2001). Aberrant lipid organization in stratum corneum of patients with atopic dermatitis and lamellar ichthyosis. *The Journal of Investigative Dermatology*, *117*(3), 710–717. https://doi.org/10.1046/j.0022-202x.2001.01455.x

Raabe, G. (2017). Molecular Dynamics Simulations. In G. Raabe (Ed.), *Molecular Simulation Studies on Thermophysical Properties: With Application to Working Fluids* (pp. 83–113). Springer Singapore. https://doi.org/10.1007/978-981-10-3545-6_4

Rapaport, D. C. (2003). An Introduction to Molecular Dynamics Simulation. In B. Dünweg, D. P. Landau, & A. I. Milchev (Eds.), *Computer Simulations of Surfaces and Interfaces* (pp. 59–73). Springer Netherlands. https://doi.org/10.1007/978-94-010-0173-1_3

Regno, A. D., & Notman, R. (2018). Permeation pathways through lateral domains in model membranes of skin lipids. *Physical Chemistry Chemical Physics*, *20*(4), 2162–2174. https://doi.org/10.1039/C7CP03258G

Rivero, N. (2019). *Estudio de dinámica molecular de un modelo de bicapa lipídica del estrato córneo constituido por CER[NP] y CER[AP]* [Tesis de Pregrado]. Universidad Industrial de Santander.

Sahle, F. F., Gebre-Mariam, T., Dobner, B., Wohlrab, J., & Neubert, R. H. H. (2015). Skin diseases associated with the depletion of stratum corneum lipids and stratum corneum lipid substitution therapy. *Skin Pharmacology and Physiology*, *28*(1), 42–55. https://doi.org/10.1159/000360009

Schmitt, T., Gupta, R., Lange, S., Sonnenberger, S., Dobner, B., Hauß, T., Rai, B., & Neubert, R. H. H. (2018). Impact of the ceramide subspecies on the nanostructure of stratum corneum lipids using neutron scattering and molecular dynamics simulations. Part I: impact of CER[NS]. *Chemistry and Physics of Lipids*, *214*, 58–68. https://doi.org/10.1016/j.chemphyslip.2018.05.006

Schmitt, T., Lange, S., Dobner, B., Sonnenberger, S., Hauß, T., & Neubert, R. H. H. (2018). Investigation of a CER[NP]- and [AP]-Based Stratum Corneum Modeling Membrane System: Using Specifically Deuterated CER Together with a Neutron Diffraction Approach. *Langmuir: The ACS Journal of Surfaces and Colloids*, *34*(4), 1742–1749. https://doi.org/10.1021/acs.langmuir.7b01848

Schmitt, T., Lange, S., Sonnenberger, S., Dobner, B., Demé, B., Neubert, R. H. H., Gooris, G., & Bouwstra, J. A. (2017). Determination of the influence of C24 D/(2R)- and L/(2S)-isomers of the CER[AP] on the lamellar structure of stratum corneum model systems using neutron diffraction. *Chemistry and Physics of Lipids*, *209*, 29–36. https://doi.org/10.1016/j.chemphyslip.2017.11.001

Schmitt, T., & Neubert, R. H. H. (2018). State of the art in Stratum Corneum research: The biophysical properties of ceramides. *Chemistry and Physics of Lipids*, *216*, 91–103. https://doi.org/10.1016/j.chemphyslip.2018.09.017

Shen, C.-P., Zhao, M.-T., Jia, Z.-X., Zhang, J.-L., Jiao, L., & Ma, L. (2018). Skin Ceramide Profile in Children With Atopic Dermatitis. *Dermatitis: Contact, Atopic, Occupational, Drug*, *29*(4), 219–222. https://doi.org/10.1097/DER.0000000000000392

Starr, N. J., Johnson, D. J., Wibawa, J., Marlow, I., Bell, M., Barrett, D. A., & Scurr, D. J. (2016). Age-Related Changes to Human Stratum Corneum Lipids Detected Using Time-of-Flight

Secondary Ion Mass Spectrometry Following in Vivo Sampling. *Analytical Chemistry*, *88*(8), 4400–4408. https://doi.org/10.1021/acs.analchem.5b04872

Sugita, Y., & Okamoto, Y. (1999). Replica-exchange molecular dynamics method for protein folding. *Chemical Physics Letters*, *314*(1), 141–151. https://doi.org/10.1016/S0009-2614(99)01123-9

Torrie, G. M., & Valleau, J. P. (1977). Nonphysical sampling distributions in Monte Carlo free-energy estimation: Umbrella sampling. *Journal of Computational Physics*, *23*(2), 187–199. https://doi.org/10.1016/0021-9991(77)90121-8

Uchida, Y., & Park, K. (2016). Stratum Corneum. *Immunology of the Skin*, 15–30. https://doi.org/10.1007/978-4-431-55855-2_2

Uline, M. J., & Corti, D. S. (2013). Molecular Dynamics at Constant Pressure: Allowing the System to Control Volume Fluctuations via a "Shell" Particle. *Entropy*, *15*(9), 3941–3969. https://doi.org/10.3390/e15093941

van der Spoel, D., van Maaren, P. J., Larsson, P., & Tîmneanu, N. (2006). Thermodynamics of Hydrogen Bonding in Hydrophilic and Hydrophobic Media. *The Journal of Physical Chemistry B*, *110*(9), 4393–4398. https://doi.org/10.1021/jp0572535

van Smeden, J., Janssens, M., Boiten, W. A., van Drongelen, V., Furio, L., Vreeken, R. J., Hovnanian, A., & Bouwstra, J. A. (2014). Intercellular skin barrier lipid composition and organization in Netherton syndrome patients. *The Journal of Investigative Dermatology*, *134*(5), 1238–1245. https://doi.org/10.1038/jid.2013.517

van Smeden, J., Janssens, M., Gooris, G. S., & Bouwstra, J. A. (2014). The important role of stratum corneum lipids for the cutaneous barrier function. *Biochimica Et Biophysica Acta*, *1841*(3), 295–313. https://doi.org/10.1016/j.bbalip.2013.11.006

Wang, E., & Klauda, J. B. (2017). Molecular Dynamics Simulations of Ceramide and Ceramide-Phosphatidylcholine Bilayers. *The Journal of Physical Chemistry. B*, *121*(43), 10091–10104. https://doi.org/10.1021/acs.jpcb.7b08967

Wefers, H., Melnik, B. C., Flür, M., Bluhm, C., Lehmann, P., & Plewig, G. (1991). Influence of UV irradiation on the composition of human stratum corneum lipids. *The Journal of Investigative Dermatology*, *96*(6), 959–962. https://doi.org/10.1111/1523-1747.ep12476124

Yamamoto, A., Serizawa, S., Ito, M., & Sato, Y. (1991). Stratum corneum lipid abnormalities in atopic dermatitis. *Archives of Dermatological Research*, *283*(4), 219–223. https://doi.org/10.1007/BF01106105

Zhou, M., Gan, Y., He, C., Chen, Z., & Jia, Y. (2018). Lipidomics reveals skin surface lipid abnormity in acne in young men. *The British Journal of Dermatology*, *179*(3), 732–740. https://doi.org/10.1111/bjd.16655

Appendices

Appendix A

Input file for building the CER[NP]:CER[AP] 1:2 model.

```
#
# CER[NP]:CER[AP] 1:2 model
#

# Every atom from different molecules will be far from each other at
# least 1.8 Angstroms at the solution.

tolerance 1.8

# Coordinate file types will be in pdb format.

filetype pdb

# The output pdb file

output 3BLNP11AP22.pdb

# Water molecules below the lipids:
# The first three numbers are the minimum x, y, z coordinates for this
# molecules, the last three are maximum coordinates. The box defined
# here has 60. Angstrom sides in the x and y directions, and a 16.
# Angstrom side in the z direction.

structure water.pdb
  number 2150
  inside box 0. 0. -16. 60. 60. 0.
end structure

# Water molecules over the lipids:
# The same as the input above, but the box of water molecules will be
# placed in a different region of space.

structure water.pdb
  number 2150
  inside box 0. 0. 160. 60. 60. 176.
end structure

# First lipid layer: the polar head is oriented to down to the water
# molecules.
# 50 lipids will be put inside a box of side 60. in the x and y
# directions and 26. in the z direction (26 is a little more than that
# length of the CERs). For example, the atoms 1 and 3 of the pdb file of
# CER[NP], which belong to the polar head, will be constrained to be
# below the the plane z = 2., and the atoms 121 and 124, which are the
# hydrophobic end of the lipid will be constrained to be over the plane
```

```
# z = 24. Therefore, all the lipids will be oriented, with their polar
# heads pointing to the water box below.

structure NP.pdb
  number 11
  inside box 0. 0. 0. 60. 60. 26.
  atoms 1 3
    below plane 0. 0. 1. 2.
  end atoms
  atoms 121 124
    over plane 0. 0. 1. 24.
  end atoms
end structure

structure NP.pdb
  number 11
  inside box 0. 0. 26. 60. 60. 52.
  atoms 121 124
    below plane 0. 0. 1. 28.
  end atoms
  atoms 1 3
    over plane 0. 0. 1. 50
  end atoms
end structure

structure AP.pdb
  number 22
  inside box 0. 0. 0. 60. 60. 26.
  atoms 1 3
    below plane 0. 0. 1. 2.
  end atoms
  atoms 121 124
    over plane 0. 0. 1. 24.
  end atoms
end structure

structure AP.pdb
  number 22
  inside box 0. 0. 26. 60. 60. 52.
  atoms 121 124
    below plane 0. 0. 1. 28.
  end atoms
  atoms 1 3
    over plane 0. 0. 1. 50
  end atoms
end structure

structure LA.pdb
  number 33
  inside box 0. 0. 0. 60. 60. 26.
  atoms 1 2
    below plane 0. 0. 1. 2.
```

```
  end atoms
  atoms 71 72
    over plane 0. 0. 1. 24.
  end atoms
end structure

structure LA.pdb
  number 33
  inside box 0. 0. 26. 60. 60. 52.
  atoms 71 72
    below plane 0. 0. 1. 28.
  end atoms
  atoms 1 2
    over plane 0. 0. 1. 50
  end atoms
end structure

structure CHL.pdb
  number 23
  inside box 0. 0. 0. 60. 60. 26.
  atoms 1 3
    below plane 0. 0. 1. 10.
  end atoms
  atoms 67 71
    over plane 0. 0. 1. 24.
  end atoms
end structure

structure CHL.pdb
  number 23
  inside box 0. 0. 26. 60. 60. 52.
  atoms 67 71
    below plane 0. 0. 1. 28.
  end atoms
  atoms 1 3
    over plane 0. 0. 1. 42
  end atoms
end structure

# Water molecules are added in the middle of monolayers.

structure water.pdb
  number 178
  inside box 0. 0. 52. 60. 60. 54.
end structure

# Second lipid layer: the polar head points up to the water molecules.
# The same thing as the input above, but defining a new lipid layer,
# with the oposite orientation of the lipid molecules in such a way that
# the polar head points to the water box that is over the lipid bilayer.

structure NP.pdb
```

```
  number 11
  inside box 0. 0. 54. 60. 60. 80.
  atoms 1 3
    below plane 0. 0. 1. 56.
  end atoms
  atoms 121 124
    over plane 0. 0. 1. 78.
  end atoms
end structure

structure NP.pdb
  number 11
  inside box 0. 0. 80. 60. 60. 106.
  atoms 121 124
    below plane 0. 0. 1. 82.
  end atoms
  atoms 1 3
    over plane 0. 0. 1. 104
  end atoms
end structure

structure AP.pdb
  number 22
  inside box 0. 0. 54. 60. 60. 80.
  atoms 1 3
    below plane 0. 0. 1. 56.
  end atoms
  atoms 121 124
    over plane 0. 0. 1. 78.
  end atoms
end structure

structure AP.pdb
  number 22
  inside box 0. 0. 80. 60. 60. 106.
  atoms 121 124
    below plane 0. 0. 1. 82.
  end atoms
  atoms 1 3
    over plane 0. 0. 1. 104
  end atoms
end structure

structure LA.pdb
  number 33
  inside box 0. 0. 54. 60. 60. 80.
  atoms 1 2
    below plane 0. 0. 1. 56.
  end atoms
  atoms 71 72
    over plane 0. 0. 1. 78.
  end atoms
```

```
end structure

structure LA.pdb
  number 33
  inside box 0. 0. 80. 60. 60. 106.
  atoms 71 72
    below plane 0. 0. 1. 82.
  end atoms
  atoms 1 2
    over plane 0. 0. 1. 104
  end atoms
end structure

structure CHL.pdb
  number 23
  inside box 0. 0. 54. 60. 60. 80.
  atoms 1 3
    below plane 0. 0. 1. 64.
  end atoms
  atoms 67 71
    over plane 0. 0. 1. 78.
  end atoms
end structure

structure CHL.pdb
  number 23
  inside box 0. 0. 80. 60. 60. 106.
  atoms 67 71
    below plane 0. 0. 1. 90.
  end atoms
  atoms 1 3
    over plane 0. 0. 1. 104
  end atoms
end structure

# Water molecules are added between monolayers and the third bilayer is built.

structure water.pdb
  number 178
  inside box 0. 0. 106. 60. 60. 108.
end structure

structure NP.pdb
  number 11
  inside box 0. 0. 108. 60. 60. 134.
  atoms 1 3
    below plane 0. 0. 1. 110.
  end atoms
  atoms 121 124
    over plane 0. 0. 1. 132.
  end atoms
end structure
```

```
structure NP.pdb
  number 11
  inside box 0. 0. 134. 60. 60. 160.
  atoms 121 124
    below plane 0. 0. 1. 136.
  end atoms
  atoms 1 3
    over plane 0. 0. 1. 158
  end atoms
end structure

structure AP.pdb
  number 22
  inside box 0. 0. 108. 60. 60. 134.
  atoms 1 3
    below plane 0. 0. 1. 110.
  end atoms
  atoms 121 124
    over plane 0. 0. 1. 132.
  end atoms
end structure

structure AP.pdb
  number 22
  inside box 0. 0. 134. 60. 60. 160.
  atoms 121 124
    below plane 0. 0. 1. 136.
  end atoms
  atoms 1 3
    over plane 0. 0. 1. 158
  end atoms
end structure

structure LA.pdb
  number 33
  inside box 0. 0. 108. 60. 60. 134.
  atoms 1 2
    below plane 0. 0. 1. 110.
  end atoms
  atoms 71 72
    over plane 0. 0. 1. 132.
  end atoms
end structure

structure LA.pdb
  number 33
  inside box 0. 0. 134. 60. 60. 160.
  atoms 71 72
    below plane 0. 0. 1. 136.
  end atoms
  atoms 1 2
```

```
    over plane 0. 0. 1. 158
  end atoms
end structure

structure CHL.pdb
  number 23
  inside box 0. 0. 108. 60. 60. 134.
  atoms 1 3
    below plane 0. 0. 1. 118.
  end atoms
  atoms 67 71
    over plane 0. 0. 1. 132.
  end atoms
end structure

structure CHL.pdb
  number 23
  inside box 0. 0. 134. 60. 60. 160.
  atoms 67 71
    below plane 0. 0. 1. 144.
  end atoms
  atoms 1 3
    over plane 0. 0. 1. 158
  end atoms
end structure
```

Appendix B

Determination of contact or overlapping.

Graphical explanation

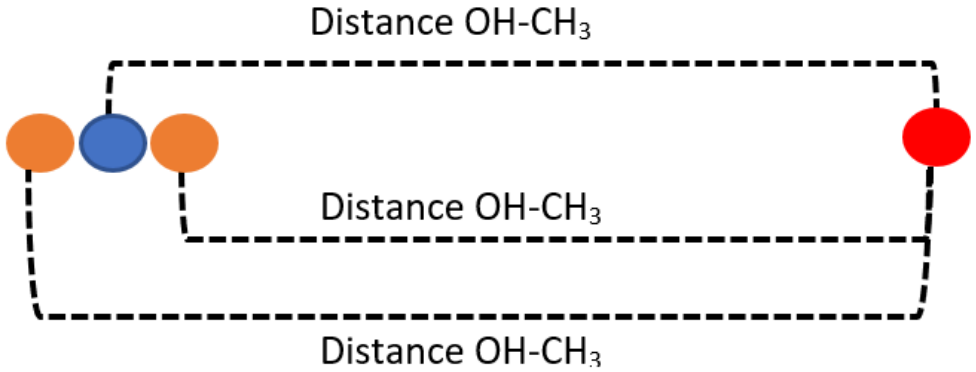

Result

Overlapping:

Distance **OH**-**CH3** on the same monolayer > Distance **OH**-**CH3** on the opposite monolayer

Contact:

Distance **OH**-**CH3** on the same monolayer < Distance **OH**-**CH3** on the opposite monolayer

Appendix C

Total lipid mass density profiles of each bilayer.

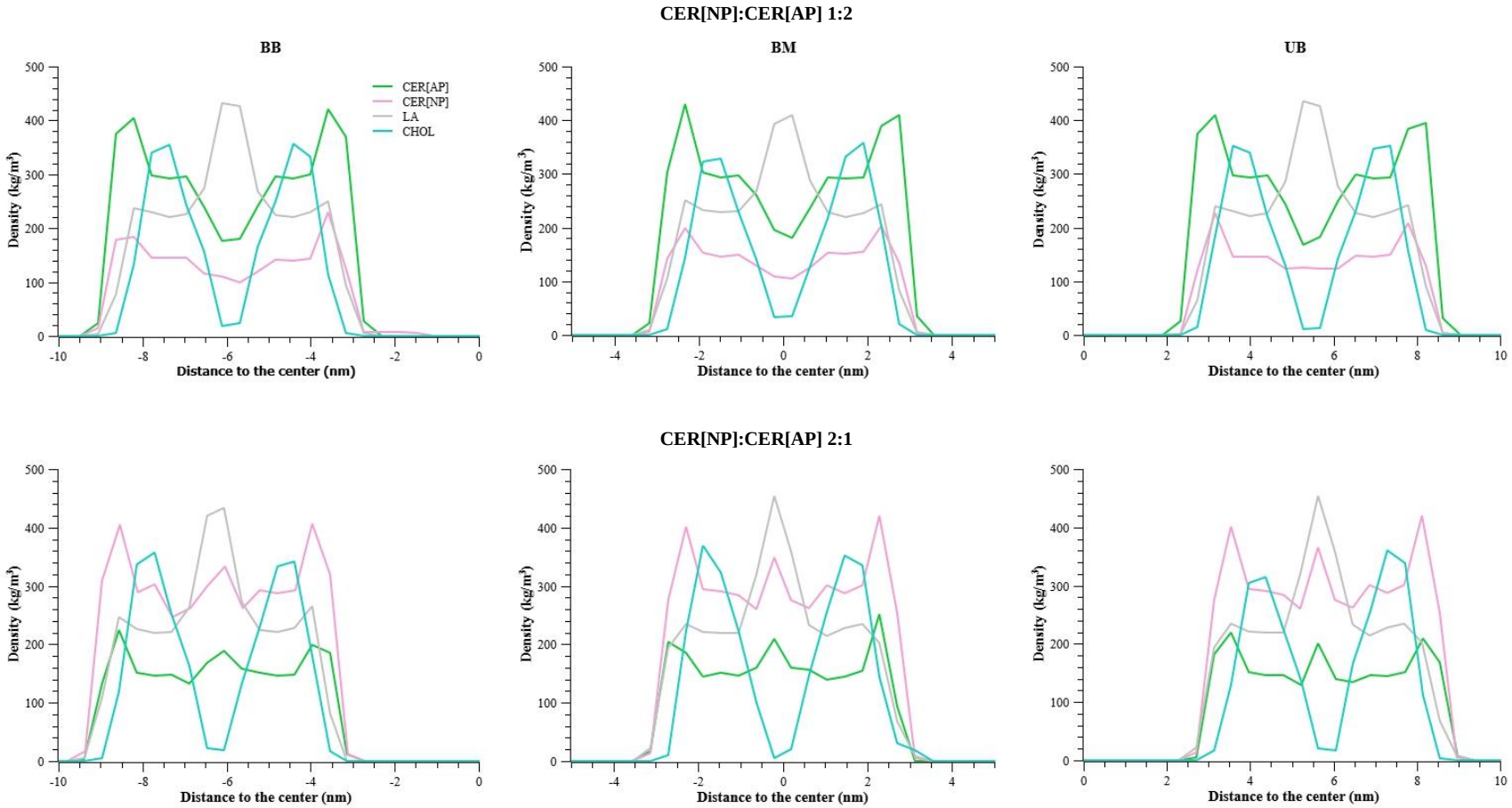

Appendix D

Histogram of the distance between the 3 -hydroxyl and the terminal CH_3 of the fatty acid chain of CER[AP] of the same monolayer and of the opposite monolayer.

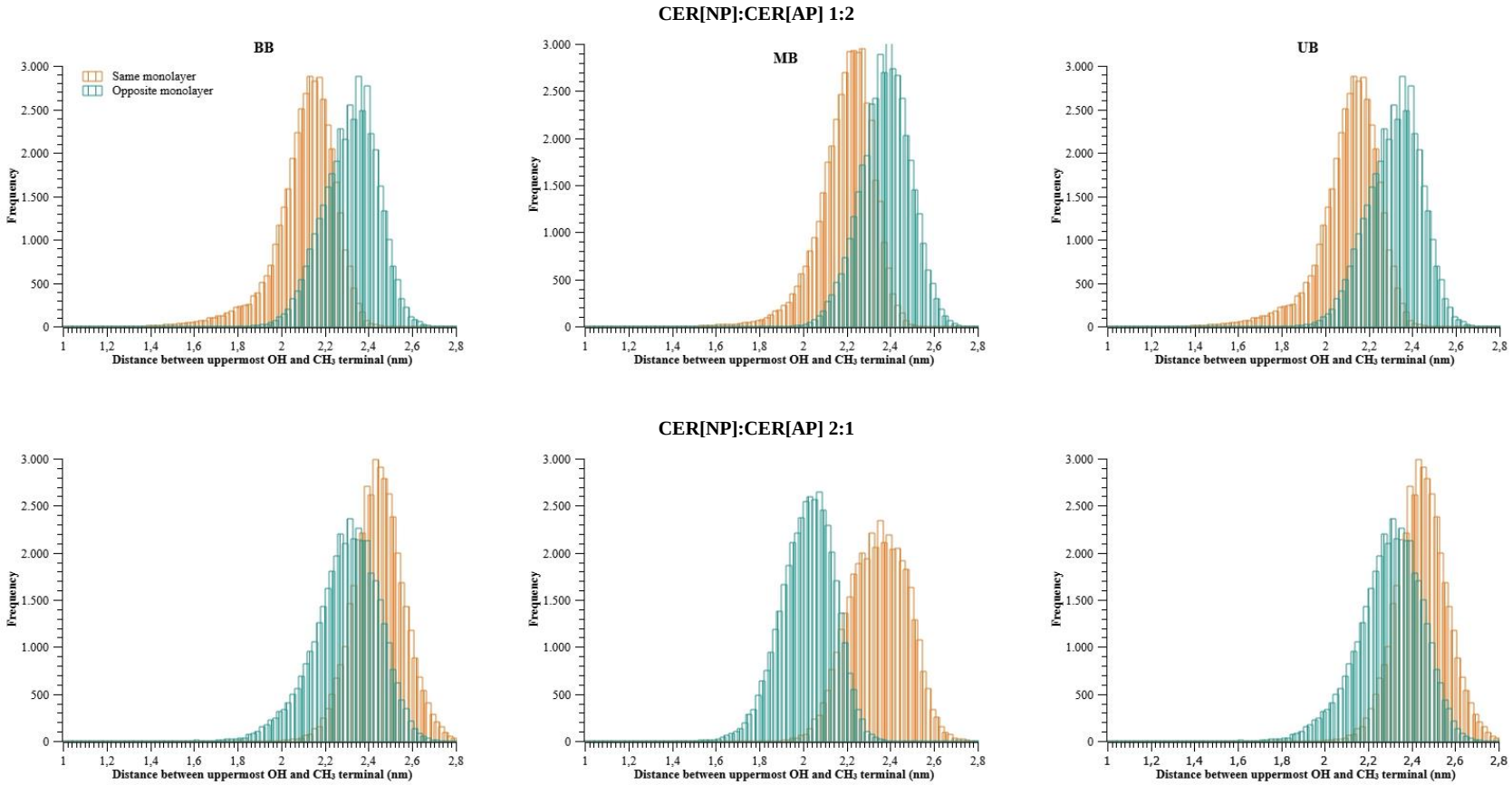

Appendix E

Histogram of the distance between the 3-hydroxyl and the terminal CH_3 of the LA chain of the same monolayer and of the opposite monolayer.

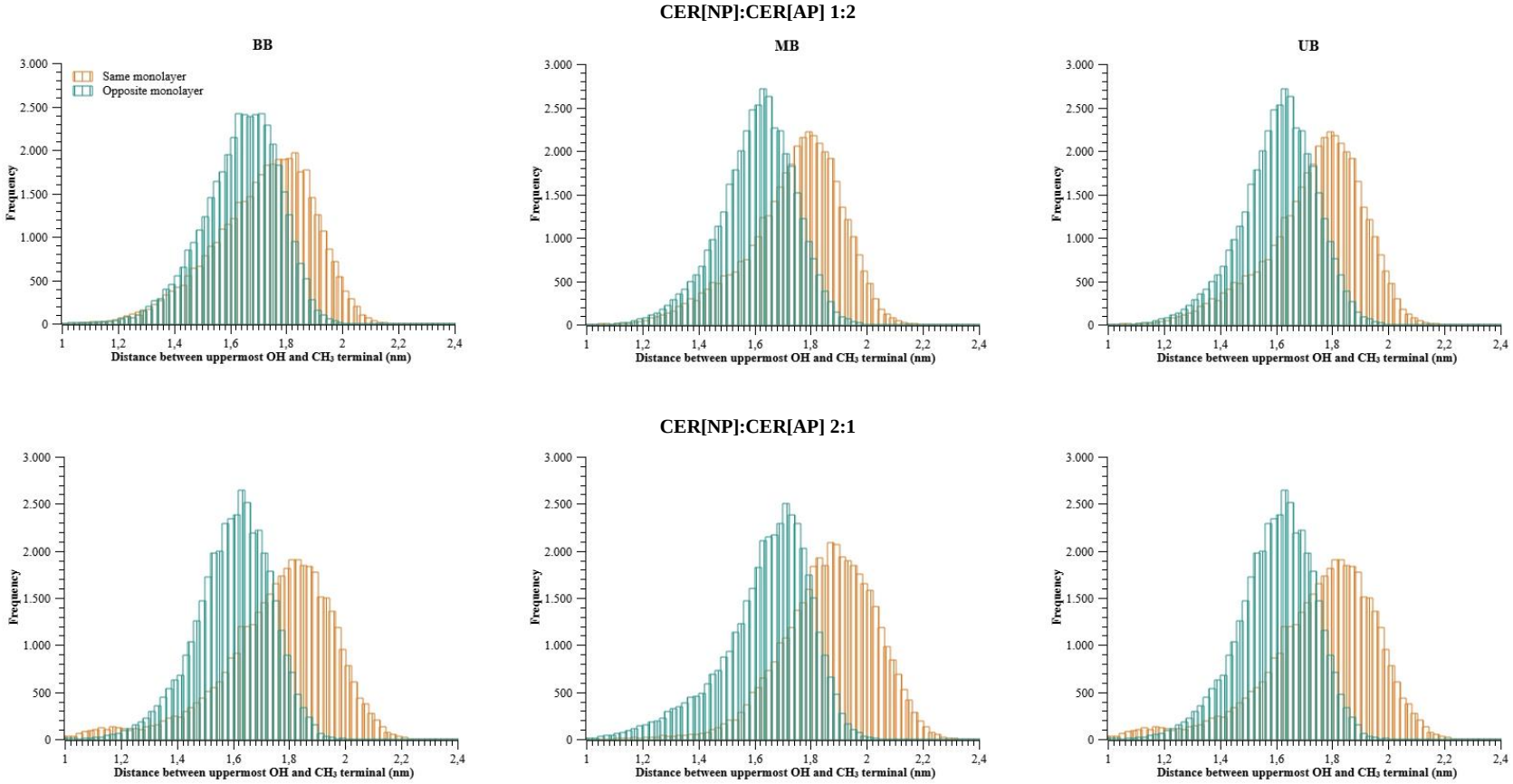

Appendix F

Histogram of the angle of inclination of the CER[AP] CER[NP] fatty acid chain and LA chain with respect to the z-axis. CER[NP]:CER[AP] 1:2 and CER[NP]:CER[AP] 2:1.

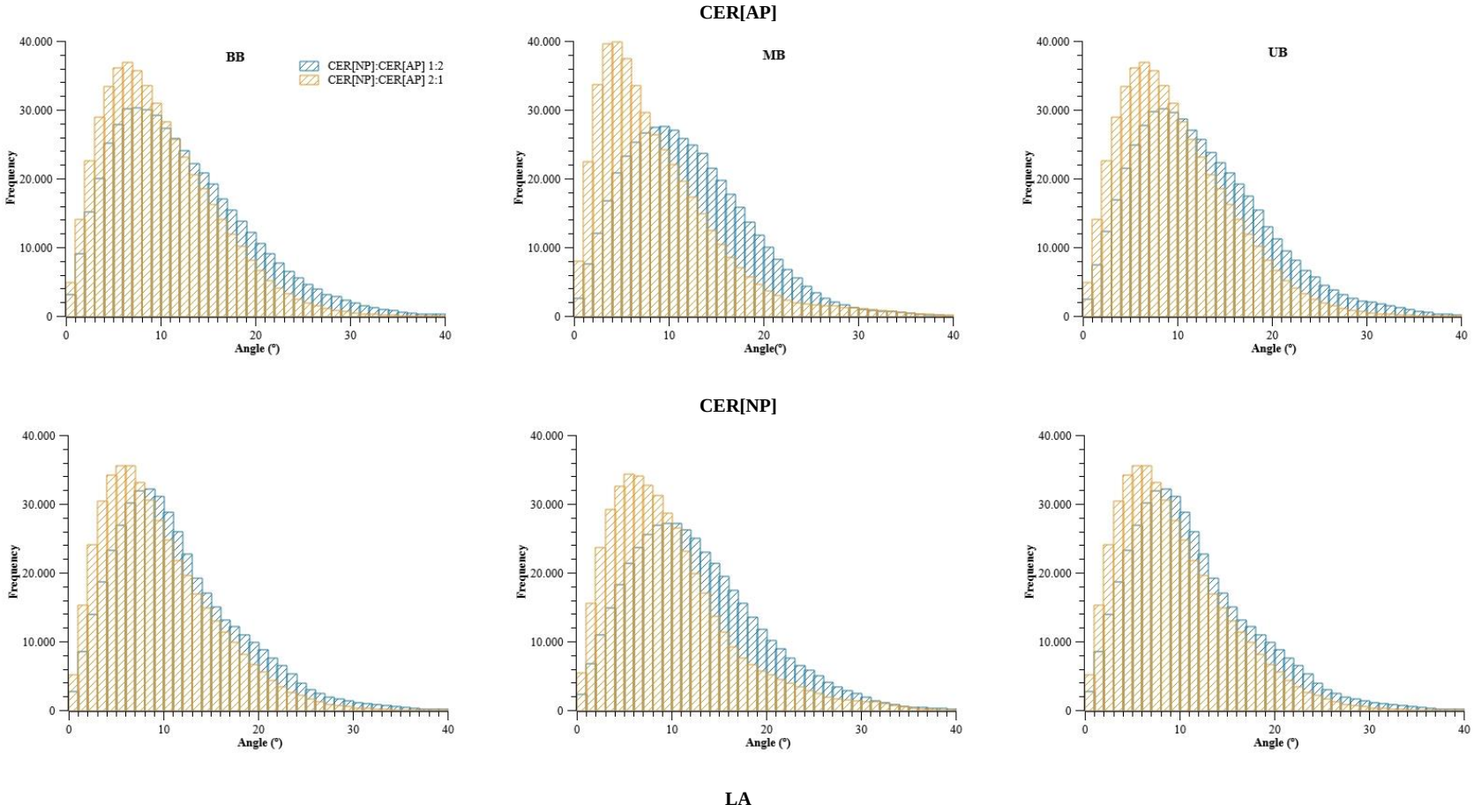

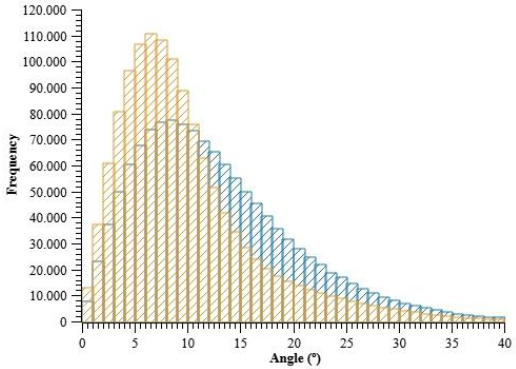
Frequency
Angle (°)

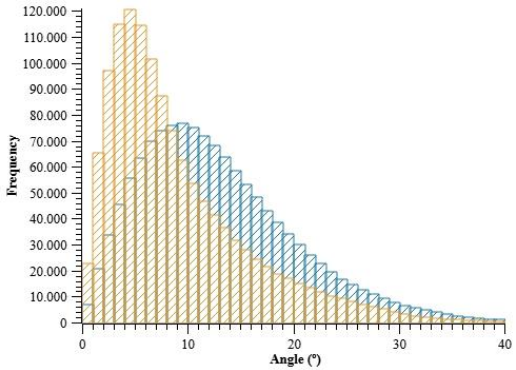
Frequency
Angle (°)

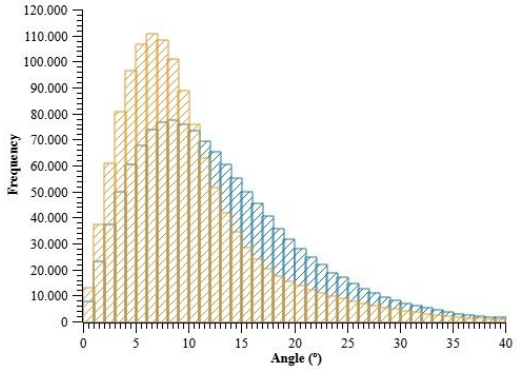
Frequency
Angle (°)

Appendix G

Most common intermolecular and intramolecular interactions formed. All donor and acceptor groups are listed with the number of hydrogen bonds formed between them per CER molecule. Calculated in the complete models, i.e., in the three stacked bilayers. Highest values are highlighted in red, medium values in yellow and lowest values in green.

Only the intermolecular interactions in the whole model

CER	Acceptors	Donors																							
		CER[AP]										CER[NP]								LA		CHOL		Water	
		H-Hydroxyl 1		H-Hydroxyl 2		H-Hydroxyl 3		H-N		H-Fatty Acid Hydroxyl		H-Hydroxyl 1		H-Hydroxyl 2		H-Hydroxyl 3		H-N		H-Hydroxyl		H-Hydroxyl			
		1:2	2:1	1:2	2:1	1:2	2:1	1:2	2:1	1:2	2:1	1:2	2:1	1:2	2:1	1:2	2:1	1:2	2:1	1:2	2:1	1:2	2:1	1:2	2:1
CER[AP]	O-Hydroxyl 1	0.06	0.17	0.05	0.11	0.03	0.02	0.10	0.10	0.05	0.03	0.06	0.01	0.05	0.02	0.04	0.02	0.01	0.02	0.03	0.01	0.06	0.02	0.01	0.00
	O-Hydroxyl 2	0.06	0.15	0.10	0.07	0.06	0.03	0.05	0.02	0.08	0.06	0.04	0.02	0.06	0.01	0.05	0.02	0.03	0.02	0.04	0.01	0.04	0.02	0.01	0.00
	O-Hydroxyl 3	0.05	0.04	0.08	0.03	0.09	0.03	0.05	0.02	0.09	0.06	0.03	0.01	0.05	0.02	0.06	0.05	0.02	0.01	0.06	0.03	0.05	0.02	0.02	0.01
	N	0.03	0.02	0.01	0.01	0.01	0.00	0.00	0.00	0.02	0.01	0.00	0.00	0.01	0.00	0.01	0.01	0.00	0.00	0.01	0.00	0.01	0.00	0.00	0.00
	O-Carbonyl	0.03	0.02	0.07	0.10	0.09	0.06	0.13	0.08	0.09	0.03	0.02	0.01	0.06	0.01	0.09	0.05	0.04	0.01	0.06	0.04	0.07	0.04	0.02	0.00
	O- Fatty Acid Hydroxyl	0.05	0.03	0.08	0.04	0.08	0.04	0.07	0.09	0.08	0.07	0.05	0.01	0.08	0.02	0.08	0.03	0.05	0.02	0.05	0.03	0.04	0.03	0.02	0.01
CER[NP]	O-Hydroxyl 1	0.02	0.04	0.01	0.03	0.02	0.04	0.03	0.03	0.03	0.02	0.04	0.10	0.01	0.07	0.02	0.03	0.07	0.14	0.02	0.02	0.02	0.05	0.00	0.00
	O-Hydroxyl 2	0.03	0.06	0.03	0.05	0.03	0.05	0.02	0.03	0.04	0.04	0.03	0.10	0.01	0.06	0.03	0.06	0.03	0.07	0.03	0.05	0.02	0.03	0.01	0.01
	O-Hydroxyl 3	0.01	0.03	0.03	0.06	0.03	0.09	0.03	0.04	0.01	0.05	0.02	0.04	0.04	0.09	0.07	0.11	0.01	0.07	0.03	0.04	0.01	0.03	0.01	0.02
	N	0.00	0.01	0.01	0.00	0.01	0.01	0.00	0.00	0.01	0.01	0.20	0.03	0.10	0.01	0.00	0.02	0.00	0.01	0.00	0.00	0.00	0.00	0.00	0.00
	O-Carbonyl	0.03	0.01	0.03	0.04	0.03	0.07	0.02	0.09	0.04	0.05	0.01	0.06	0.03	0.07	0.05	0.11	0.09	0.15	0.03	0.04	0.06	0.08	0.01	0.02

LA	**O-Hydroxyl**	0.05	0.02	0.05	0.03	0.04	0.05	0.02	0.02	0.06	0.07	0.07	0.03	0.05	0.04	0.04	0.03	0.04	0.02	0.03	0.06	0.02	0.03	0.01	0.01
	O-Carbonyl	0.16	0.08	0.07	0.05	0.09	0.09	0.11	0.12	0.10	0.11	0.23	0.15	0.09	0.07	0.70	0.05	0.12	0.09	0.06	0.15	0.07	0.07	0.02	0.02
CHOL	**OH**	0.08	0.06	0.03	0.03	0.09	0.06	0.08	0.07	0.05	0.06	0.04	0.07	0.03	0.03	0.05	0.05	0.06	0.06	0.03	0.05	0.01	0.01	0.02	0.03
Water		0.29	0.23	0.41	0.41	0.87	0.94	0.39	0.39	0.56	0.60	0.28	0.27	0.51	0.49	0.90	0.90	0.40	0.32	0.86	0.83	0.86	0.93	2.02	2.02
Sum			**0.95**		**1.06**		**1.57**		**1.10**		**1.29**		**0.92**		**1.04**		**1.55**		**0.98**		**1.37**		**1.37**		**2.18**

Only the intramolecular interactions in the whole model

		Donors																							
		CER[AP]										CER[NP]								LA		CHOL		Water	
CER	Acceptors	H-Hydroxyl 1		H-Hydroxyl 2		H-Hydroxyl 3		H-N		H- Fatty Acid Hydroxyl		H-Hydroxyl 1		H-Hydroxyl 2		H-Hydroxyl 3		H-N		H-Hydroxyl		H-Hydroxyl			
		1:2	2:1	1:2	2:1	1:2	2:1	1:2	2:1	1:2	2:1	1:2	2:1	1:2	2:1	1:2	2:1	1:2	2:1	1:2	2:1	1:2	2:1	1:2	2:1
CER[AP]	O-Hydroxyl 1	0.00	0.00	0.21	0.19	0.00	0.00	0.21	0.22	0.00	0.00	0.00	0.00	0.00	0.00	0.00	0.00	0.00	0.00	0.00	0.00	0.00	0.00	0.00	0.00
	O-Hydroxyl 2	0.45	0.42	0.00	0.00	0.05	0.07	0.04	0.02	0.00	0.00	0.00	0.00	0.00	0.00	0.00	0.00	0.00	0.00	0.00	0.00	0.00	0.00	0.00	0.00
	O-Hydroxyl 3	0.45	0.46	0.00	0.00	0.00	0.00	0.38	0.39	0.00	0.00	0.00	0.00	0.00	0.00	0.00	0.00	0.00	0.00	0.00	0.00	0.00	0.00	0.00	0.00
	N	0.13	0.10	0.02	0.01	0.13	0.10	0.00	0.00	0.01	0.01	0.00	0.00	0.00	0.00	0.00	0.00	0.00	0.00	0.00	0.00	0.00	0.00	0.00	0.00
	O-Carbonyl	0.12	0.11	0.00	0.00	0.02	0.02	0.00	0.00	0.46	0.49	0.00	0.00	0.00	0.00	0.00	0.00	0.00	0.00	0.00	0.00	0.00	0.00	0.00	0.00
	O- Fatty Acid Hydroxyl	0.00	0.00	0.00	0.00	0.00	0.00	0.05	0.05	0.00	0.00	0.00	0.00	0.00	0.00	0.00	0.00	0.00	0.00	0.00	0.00	0.00	0.00	0.00	0.00
CER[NP]	O-Hydroxyl 1	0.00	0.00	0.00	0.00	0.00	0.00	0.00	0.00	0.00	0.00	0.00	0.00	0.22	0.22	0.00	0.00	0.36	0.31	0.00	0.00	0.00	0.00	0.00	0.00

	O-Hydroxyl 2	0.00	0.00	0.00	0.00	0.00	0.00	0.00	0.00	0.00	0.00	0.27	0.34	0.00	0.00	0.06	0.06	0.03	0.01	0.00	0.00	0.00	0.00	0.00	0.00		
	O-Hydroxyl 3	0.00	0.00	0.00	0.00	0.00	0.00	0.00	0.00	0.00	0.00	0.00	0.00	0.43	0.46	0.00	0.00	0.34	0.37	0.00	0.00	0.00	0.00	0.00	0.00		
	N	0.00	0.00	0.00	0.00	0.00	0.00	0.00	0.00	0.00	0.00	0.10	0.09	0.03	0.01	0.14	0.02	0.00	0.00	0.00	0.00	0.00	0.00	0.00	0.00		
	O-Carbonyl	0.00	0.00	0.00	0.00	0.00	0.00	0.00	0.00	0.00	0.00	0.12	0.11	0.00	0.00	0.02	0.01	0.00	0.00	0.00	0.00	0.00	0.00	0.00	0.00		

Appendix H

Most common intermolecular and intramolecular interactions formed. All donor and acceptor groups are listed with the number of hydrogen bonds formed between them per CER molecule. Calculated only in the central bilayer including the neighboring monolayers. Highest values are highlighted in red, medium values in yellow and lowest values in green.

Only the intermolecular interactions in the whole model

CER	Acceptors	Donors																							
		CER[AP]										CER[NP]								LA		CHOL		Water	
		H-Hydroxyl 1		H-Hydroxyl 2		H-Hydroxyl 3		H-N		H- Fatty Acid Hydroxyl		H-Hydroxyl 1		H-Hydroxyl 2		H-Hydroxyl 3		H-N		H-Hydroxyl		H-Hydroxyl			
		1:2	2:1	1:2	2:1	1:2	2:1	1:2	2:1	1:2	2:1	1:2	2:1	1:2	2:1	1:2	2:1	1:2	2:1	1:2	2:1	1:2	2:1	1:2	2:1
CER[AP]	O-Hydroxyl 1	0.06	0.19	0.05	0.12	0.04	0.01	0.09	0.10	0.06	0.03	0.05	0.02	0.05	0.02	0.06	0.03	0.03	0.01	0.05	0.01	0.04	0.03	0.09	0.03
	O-Hydroxyl 2	0.05	0.17	0.07	0.05	0.06	0.03	0.04	0.02	0.09	0.07	0.04	0.03	0.08	0.02	0.06	0.03	0.01	0.01	0.04	0.01	0.07	0.03	0.08	0.03
	O-Hydroxyl 3	0.05	0.04	0.07	0.03	0.10	0.03	0.06	0.02	0.12	0.08	0.04	0.01	0.07	0.02	0.09	0.07	0.03	0.02	0.08	0.04	0.07	0.02	0.11	0.06
	N	0.02	0.02	0.01	0.01	0.02	0.00	0.00	0.00	0.02	0.03	0.01	0.00	0.01	0.00	0.01	0.00	0.00	0.01	0.01	0.00	0.01	0.01	0.02	0.01
	O-Carbonyl	0.03	0.01	0.09	0.11	0.12	0.07	0.11	0.07	0.12	0.03	0.02	0.01	0.06	0.03	0.13	0.07	0.05	0.01	0.08	0.05	0.09	0.06	0.14	0.07
	O- Fatty Acid Hydroxyl	0.06	0.03	0.09	0.05	0.12	0.05	0.09	0.12	0.12	0.06	0.05	0.02	0.07	0.02	0.11	0.05	0.05	0.02	0.07	0.04	0.05	0.03	0.10	0.06

CER[NP]	O-Hydroxyl 1	0.02	0.05	0.01	0.03	0.02	0.05	0.02	0.01	0.02	0.03	0.02	0.10	0.01	0.07	0.03	0.04	0.09	0.16	0.03	0.03	0.03	0.05	0.04	0.07
	O-Hydroxyl 2	0.03	0.08	0.03	0.04	0.04	0.05	0.02	0.02	0.04	0.04	0.03	0.10	0.01	0.07	0.04	0.07	0.04	0.06	0.01	0.05	0.01	0.04	0.02	0.10
	O-Hydroxyl 3	0.03	0.02	0.02	0.07	0.04	0.12	0.02	0.05	0.03	0.07	0.03	0.05	0.06	0.11	0.10	0.14	0.02	0.08	0.04	0.06	0.02	0.04	0.06	0.11
	N	0.00	0.00	0.01	0.00	0.01	0.02	0.00	0.00	0.01	0.01	0.02	0.03	0.01	0.01	0.01	0.02	0.00	0.01	0.00	0.01	0.00	0.01	0.01	0.02
	O-Carbonyl	0.02	0.01	0.03	0.05	0.04	0.10	0.02	0.06	0.03	0.06	0.01	0.05	0.04	0.08	0.07	0.15	0.12	0.17	0.04	0.05	0.06	0.09	0.05	0.10
LA	O-Hydroxyl	0.05	0.02	0.05	0.04	0.07	0.07	0.03	0.02	0.06	0.07	0.06	0.04	0.06	0.05	0.05	0.04	0.04	0.02	0.04	0.08	0.03	0.03	0.09	0.08
	O-Carbonyl	0.15	0.07	0.09	0.06	0.13	0.13	0.14	0.12	0.11	0.13	0.21	0.17	0.09	0.08	0.09	0.07	0.11	0.08	0.08	0.19	0.08	0.08	0.11	0.16
CHOL	OH	0.10	0.06	0.04	0.04	0.13	0.10	0.04	0.07	0.08	0.09	0.05	0.07	0.04	0.04	0.07	0.07	0.08	0.06	0.04	0.06	0.01	0.01	0.18	0.20
Water		0.28	0.19	0.36	0.35	0.58	0.72	0.34	0.37	0.40	0.51	0.26	0.24	0.43	0.40	0.61	0.63	0.35	0.27	0.72	0.67	0.77	0.83	0.82	0.87
Sum		**0.95**	**0.96**	**1.02**	**1.05**	**1.52**	**1.55**	**1.02**	**1.05**	**1.31**	**1.31**	**0.90**	**0.94**	**1.09**	**1.02**	**1.53**	**1.48**	**1.02**	**0.99**	**1.33**	**1.35**	**1.34**	**1.36**	**1.92**	**1.97**

Only the intramolecular interactions in the whole model

CER	Acceptors	Donors																							
		CER[AP]										CER[NP]								LA		CHOL		Water	
		H-Hydroxyl 1		H-Hydroxyl 2		H-Hydroxyl 3		H-N		H- Fatty Acid Hydroxyl		H-Hydroxyl 1		H-Hydroxyl 2		H-Hydroxyl 3		H-N		H-Hydroxyl		H-Hydroxyl			
		1:2	2:1	1:2	2:1	1:2	2:1	1:2	2:1	1:2	2:1	1:2	2:1	1:2	2:1	1:2	2:1	1:2	2:1	1:2	2:1	1:2	2:1	1:2	2:1
CER[AP]	O-Hydroxyl 1	0.00	0.00	0.22	0.20	0.00	0.00	0.24	0.23	0.00	0.00	0.00	0.00	0.00	0.00	0.00	0.00	0.00	0.00	0.00	0.00	0.00	0.00	0.00	0.00
	O-Hydroxyl 2	0.43	0.39	0.00	0.00	0.05	0.07	0.05	0.02	0.00	0.00	0.00	0.00	0.00	0.00	0.00	0.00	0.00	0.00	0.00	0.00	0.00	0.00	0.00	0.00
	O-Hydroxyl 3	0.45	0.45	0.00	0.00	0.00	0.00	0.38	0.42	0.00	0.00	0.00	0.00	0.00	0.00	0.00	0.00	0.00	0.00	0.00	0.00	0.00	0.00	0.00	0.00
	N	0.09	0.10	0.03	0.01	0.13	0.10	0.01	0.01	0.00	0.00	0.00	0.00	0.00	0.00	0.00	0.00	0.00	0.00	0.00	0.00	0.00	0.00	0.00	0.00

	O-Carbonyl	0.12	0.12	0.00	0.00	0.02	0.02	0.00	0.00	0.48	0.50	0.00	0.00	0.00	0.00	0.00	0.00	0.00	0.00	0.00	0.00	0.00	0.00	0.00	0.00
	O- Fatty Acid Hydroxyl	0.00	0.00	0.00	0.00	0.00	0.00	0.06	0.04	0.01	0.01	0.00	0.00	0.00	0.00	0.00	0.00	0.00	0.00	0.00	0.00	0.00	0.00	0.00	0.00
CER[NP]	O-Hydroxyl 1	0.00	0.00	0.00	0.00	0.00	0.00	0.00	0.00	0.00	0.00	0.00	0.00	0.23	0.24	0.00	0.00	0.29	0.28	0.00	0.00	0.00	0.00	0.00	0.00
	O-Hydroxyl 2	0.00	0.00	0.00	0.00	0.00	0.00	0.00	0.00	0.00	0.00	0.31	0.35	0.00	0.00	0.07	0.06	0.05	0.02	0.00	0.00	0.00	0.00	0.00	0.00
	O-Hydroxyl 3	0.00	0.00	0.00	0.00	0.00	0.00	0.00	0.00	0.00	0.00	0.00	0.00	0.41	0.44	0.00	0.00	0.37	0.39	0.00	0.00	0.00	0.00	0.00	0.00
	N	0.00	0.00	0.00	0.00	0.00	0.00	0.00	0.00	0.00	0.00	0.11	0.10	0.05	0.01	0.15	0.15	0.00	0.00	0.00	0.00	0.00	0.00	0.00	0.00
	O-Carbonyl	0.00	0.00	0.00	0.00	0.00	0.00	0.00	0.00	0.00	0.00	0.13	0.12	0.00	0.00	0.02	0.02	0.00	0.00	0.00	0.00	0.00	0.00	0.00	0.00

Appendix I

Interlayer interactions formed. All donor and acceptor groups are listed with the number of hydrogen bonds formed between them per CER molecule. Calculated in the complete models, i.e., in the three stacked bilayers. Highest values are highlighted in red, medium values in yellow and lowest values in green.

Only the intermolecular interactions in the whole model																				
CER	Acceptors	Donors																		
		CER[AP]										CER[NP]								
		H-Hydroxyl 1		H-Hydroxyl 2		H-Hydroxyl 3		H-N		H- Fatty Acid Hydroxyl		H-Hydroxyl 1		H-Hydroxyl 2		H-Hydroxyl 3		H-N		
		1:2	2:1	1:2	2:1	1:2	2:1	1:2	2:1	1:2	2:1	1:2	2:1	1:2	2:1	1:2	2:1	1:2	2:1	
CER[AP]	O-Hydroxyl 1	1.0E-04	0.0E+00	2.0E-03	5.7E-04	2.0E-02	1.2E-03	6.0E-03	5.5E-07	1.0E-02	2.8E-06	7.3E-04	8.5E-06	9.2E-03	5.4E-04	2.8E-02	2.6E-02	5.6E-04	4.1E-04	
	O-Hydroxyl 2	3.0E-04	3.0E-04	4.0E-03	9.0E-05	2.0E-02	3.0E-04	6.0E-03	6.0E-06	1.0E-02	3.0E-04	1.2E-02	9.0E-05	4.4E-03	5.0E-04	2.8E-02	2.4E-02	9.4E-04	7.0E-06	
	O-Hydroxyl 3	1.0E-02	1.0E-03	2.0E-02	9.0E-04	6.0E-02	3.0E-03	3.0E-02	1.0E-05	6.0E-02	9.0E-05	2.8E-02	3.0E-03	4.2E-02	8.0E-03	5.3E-02	4.0E-02	1.2E-02	7.0E-03	
	N	1.0E-03	2.0E-05	2.0E-03	1.0E-05	1.0E-02	2.0E-03	2.0E-04	0.0E+00	1.0E-02	1.0E-05	2.5E-04	6.0E-05	3.2E-03	5.0E-04	9.6E-03	1.0E-02	4.4E-05	4.0E-03	

	O-Carbonyl	5.0E-03	5.0E-05	1.0E-02	3.0E-04	8.0E-02	5.0E-03	3.0E-02	2.0E-04	6.0E-02	1.0E-04	1.2E-02	2.0E-03	4.6E-02	6.0E-03	9.6E-02	2.0E-03	2.9E-02	4.0E-04
	O- Fatty Acid Hydroxyl	6.0E-03	4.0E-05	2.0E-02	2.0E-04	9.0E-02	3.0E-03	2.0E-02	3.0E-04	4.0E-02	9.0E-05	2.8E-03	3.0E-03	4.2E-02	8.0E-03	9.9E-02	4.0E-02	3.1E-02	7.0E-03
CER[NP]	O-Hydroxyl 1	2.5E-04	3.0E-03	2.6E-03	2.0E-04	1.9E-02	4.0E-02	1.0E-04	4.0E-04	1.3E-02	9.0E-03	2.4E-05	2.0E-04	1.2E-04	2.0E-03	4.7E-03	3.0E-02	7.0E-05	8.0E-04
	O-Hydroxyl 2	1.6E-03	6.0E-04	7.0E-03	7.0E-03	3.2E-02	4.0E-02	6.6E-03	2.0E-03	1.2E-02	9.0E-03	8.8E-04	1.0E-03	3.6E-04	6.0E-03	1.7E-02	3.0E-02	2.2E-04	2.0E-03
	O-Hydroxyl 3	7.1E-03	1.0E-02	1.0E-02	4.0E-02	2.9E-02	1.0E-01	5.7E-03	5.0E-02	2.3E-02	5.0E-02	3.5E-03	7.0E-03	1.1E-02	4.0E-02	5.9E-02	8.0E-02	1.1E-02	4.0E-02
	N	3.8E-05	7.0E-05	1.9E-04	7.0E-04	5.7E-03	1.0E-02	5.7E-04	1.1E-03	2.7E-03	5.0E-03	2.9E-03	4.0E-05	3.7E-03	1.0E-03	5.3E-02	2.0E-02	1.1E-02	8.0E-02
	O-Carbonyl	4.1E-04	3.0E-03	3.3E-04	1.0E-02	5.6E-03	1.0E-01	6.2E-03	5.0E-02	1.1E-02	5.0E-02	2.8E-05	3.0E-03	5.7E-04	2.0E-02	5.4E-03	8.0E-05	5.6E-07	7.0E-03